Volume 47 | Number 11 | 21 March 2018 | Pages 3599–4002

Dalton Transactions

An international journal of inorganic chemistry

rsc.li/dalton

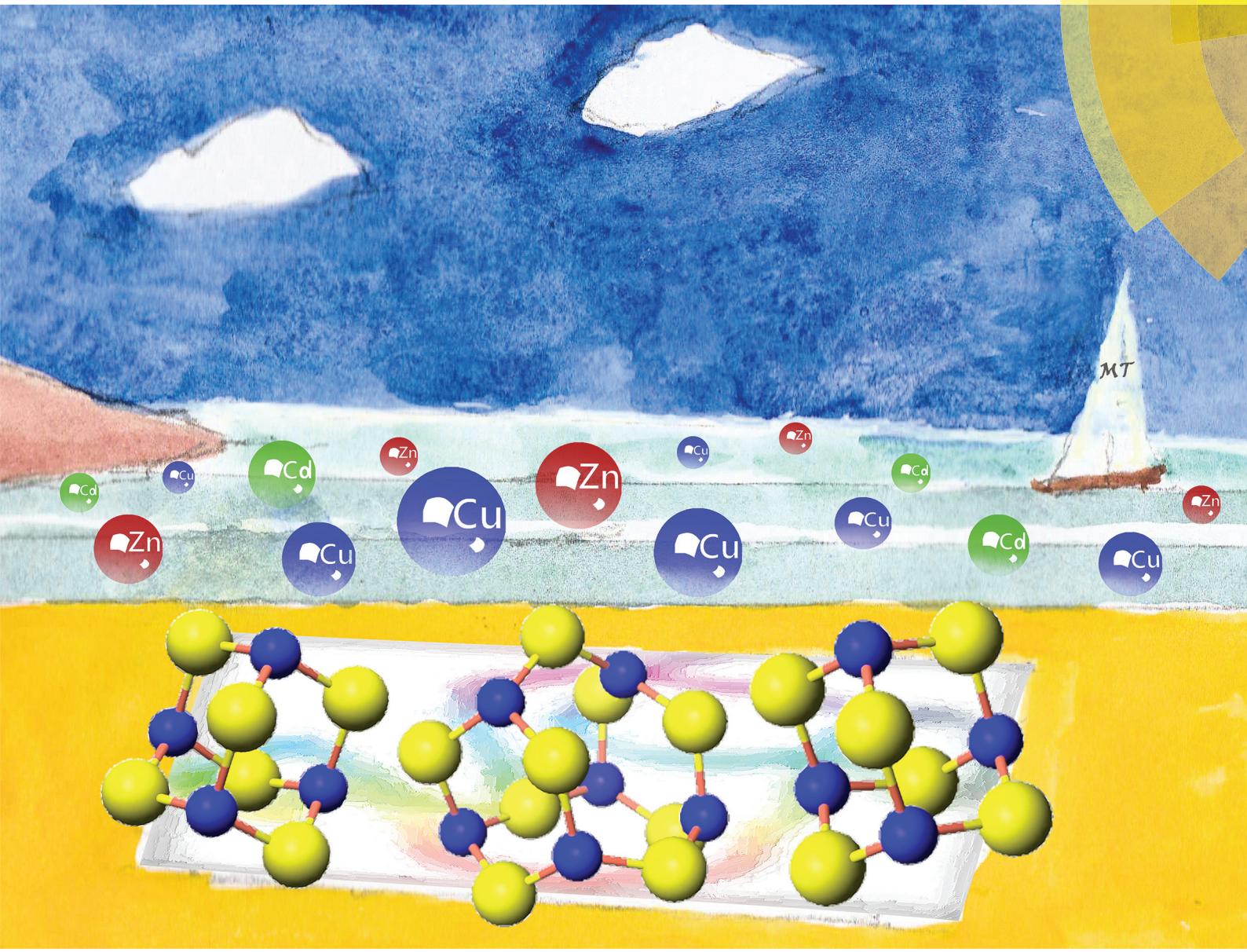

ISSN 1477-9226

ROYAL SOCIETY OF CHEMISTRY

PERSPECTIVE

Martin J. Stillman *et al.*

Unravelling the mechanistic details of metal binding to mammalian metallothioneins from stoichiometric, kinetic, and binding affinity data

Dalton Transactions

PERSPECTIVE

View Article Online
View Journal | View Issue

Check for updates

Cite this: *Dalton Trans.*, 2018, **47**, 3613

Unravelling the mechanistic details of metal binding to mammalian metallothioneins from stoichiometric, kinetic, and binding affinity data

Judith S. Scheller, Gordon W. Irvine and Martin J. Stillman *

Metallothioneins (MTs) are small, cysteine-rich proteins, found throughout Nature. Their ability to bind a number of different metals with a range of stoichiometric ratios means that this protein family is critically important for essential metal (Zn^{2+} and Cu^{+}) homeostasis, metal storage, metal donation to nascent metalloenzymes as well as heavy metal detoxification. With its 20 cysteines, metallothionein is also considered to protect cells against oxidative stress. MT has been studied by a large number of researchers over the last 6 decades using a variety of spectroscopic techniques. The lack of distinguishing chromophores for the multitude of binding sites has made the evaluation of stoichiometric properties for different metals challenging. Initially, only ^{113}Cd-NMR spectroscopy could provide strong evidence for the proposed cluster formation of Cd-MT. The extraordinary development of electrospray ionization mass spectrometry (ESI-MS), where all coexisting species in solution are observed, revolutionized MT research. Prior to the use of ESI-MS data, a range of "magic numbers" representing metal-to-MT molar ratios were reported from optical spectroscopic studies. The availability of ESI mass spectral data led to (i) the confirmation of cluster formation, (ii) a conceptual understanding of the cooperativity involved in multiple metal binding events, (iii) the presence of domain specificity between regions of the protein and (iv) mechanistic details involving both binding affinities and rate constants. The kinetic experiments identified the presence of multiple individual binding sites, each with a unique rate constant and an analogous binding affinity. The almost linear trend in rate constants as a function of bound As^{3+} provided a unique insight that became a critical step in the complete understanding of the mechanistic details of the metalation of MT. To fully define the biological function of this sulfur-rich protein it is necessary to determine kinetic rate constants and binding affinities for the essential metals. Recently, Zn^{2+} competition experiments between both of the isolated fragments (α and β) and the full-length protein (βα-MT 1a) as well as Zn^{2+} competition between βα-MT 1a and carbonic anhydrase were reported. From these data, the trend in binding affinities and the values of the K_f of the 7 bimolecular reactions involved in metalation were determined. From the analysis of ESI-MS data for Cu^{+} binding to βα-MT 1a at different pH-values, a trend in the 20 binding affinities for the complete metalation mechanism was reported. This review details a personal view of the historical development of the determination of stoichiometry for metal binding, the structure of the binding sites, the rates of the metalation reactions and the underlying binding affinities for each metalation step. We have attempted to summarize the experimental developments that led to the publication in May 2017 of the experimental determination of the 20 binding constants for the 20 sequential bimolecular reactions for Cu^{+} binding to the 20 Cys of apoMT as a function of pH that show the appearance and disappearance of clusters. We report both published data and in a series of tables an assembly of stoichiometries, and equilibrium constants for Zn^{2+} and Cu^{+} for many different metallothioneins.

Received 7th September 2017,
Accepted 26th January 2018

DOI: 10.1039/c7dt03319b

rsc.li/dalton

Open Access Article. Published on 29 ledna 2018. Downloaded on 14.02.2026 23:30:44.
This article is licensed under a Creative Commons Attribution 3.0 Unported Licence.

1. Introduction

The family of mammalian metallothioneins (MTs) is characterized by small molecular weight (6–8 kDa), high cysteine content (~30%), and the absence of disulfide bonds as well as the general lack of aromatic amino acids. MT[1–5] was first isolated in 1957 as a curious cadmium-containing protein in the horse kidney cortex.[6] MTs have now been isolated from a very large number of different organisms throughout Nature.[2,7] While mammalian MTs are the best studied MTs, plant MTs have also become a focus of great interest in recent years.[8–10] There are 4 major mammalian MT isoforms, MT1–MT4, and a

Department of Chemistry, The University of Western Ontario, London, Ontario, N6A 5B7, Canada. E-mail: martin.stillman@uwo.ca; Tel: +1-519-661-3821

Open Access Article. Published on 29 ledna 2018. Downloaded on 14.02.2026 23:30:44.
This article is licensed under a Creative Commons Attribution 3.0 Unported Licence.

number of sub-isoforms with very similar sequences. The expressions of MT1 and MT2 can be induced by a variety of factors, especially heavy metals;[11–13] MT1 is primarily found in the kidneys[14] and MT2 in the liver, but both are constitutively expressed.[15,16] The other two isoforms, MT3 and MT4, are less inducible and are found in the central nervous system[17] and the squamous epithelial tissue,[18] respectively. All four isoforms contain 20 cysteine residues, which share Cys-X-Cys, Cys-Cys or Cys-X-X-Cys metal binding motifs.[19] MT can bind a vast array of metals, essential as well as toxic, such as Zn^{2+}, Cu^{+}, Cd^{2+}, Hg^{2+} and As^{3+} to name a few. Depending on the electron configuration of the metal, stoichiometries from M_7-MT to MT_{20}-MT have been reported.[4] Its ability to bind a variety of metals, especially d^{10} metals, resulted in suggested roles in metal homeostasis and heavy metal detoxification within the cell.[20–25] It is also a proposed facilitator chaperoning metals to metal-dependent enzymes and metalloproteins,[26–28] and finally it has been suggested to be active in protecting cells against oxidative stress.[29–31] Recently, its role in intercepting metallodrugs[32] and in controlling metals in Alzheimer's disease[33] has suggested wider roles *in vitro*.

We have consulted many published resources and have referenced as many as we felt reasonable in this review to provide a general detailed insight into the complex biologically important chemistry of the metallothioneins. These reviews and research reports stretch back to the 1960 paper by Kägi and Vallee[34,35] and include the series of monographs from the Metallothionein Conferences, numerous reviews and many thousands of research publications. Here we cite a small sample that will provide the reader with guidance on both the historical developments and the current state of knowledge. The listed papers are just a small sample of those published and omission from our reference list is based on space rather than significance and we apologise to those authors of material we have omitted based simply on space restrictions.

While the majority of published reviews mostly discussed function,[11,36–38] structure[2,3,5,39–43] and/or stoichiometry,[4,44–47] we will in this review concentrate on the efforts that have been made to elucidate the metalation mechanism of MT. Recently, a long series of papers from our group have described metalation reaction rate constants and determined the individual binding constants for different metals and characterized the pH dependence of these constants.[48–55] This review concerns not only our own perspective on the determination of the individual parameters which are necessary to fully understand the binding mechanism of different metals, but also recent work, particularly concerning metalation pathways of Zn^{2+} and Cu^{+} to metallothionein. We have focused in our work on extracting binding constants from ESI-MS data. We have also extracted conformational information, especially on the partially metalated proteins, from, initially, molecular dynamics studies, and later from cysteine modification studies, where we have associated the non-normal distribution of the stepwise modification reactions as measured by ESI-MS methods with the differential shielding of cysteines as a result of folding.[43,56,57] Finally, we have over the last 20 years attempted to understand how these quite remarkable natural molecules work. While the down to earth parameters we have reported are vital parameters, as this is a Perspective review, allow me to stand in awe at these natural molecules that can twist and turn to absorb so many different metals into structures and that in many cases exceed inorganic chemistry in their complexity.

2. Metalation of metallothionein

2.1. Experimental tools

Metallothionein is an unusual protein in that it does not contain aromatic amino acids and, as a result, there is no absorption above 230 nm in the apoprotein. In addition, the

Judith S. Scheller

Ms Judith Scheller was born in Wurzburg, Germany, and received her degree in Food Chemistry from the Karlsruhe Institute of Technology (KIT), Germany, in 2016. As part of a student exchange between Prof. Dr Martin Stillman and Prof. Dr Andrea Hartwig (KIT) she conducted research in the Stillman Bioinorganic group at the University of Western Ontario, focusing on copper(I) binding to apo-metallothionein using mainly electrospray ionization mass spectrometry. She is now studying for her PhD in biochemistry at Ulm University, Ulm, Germany.

Gordon W. Irvine

Dr Gordon Irvine was born in beautiful St. Catharines, Ontario. He graduated with a PhD from Martin Stillman's group at the University of Western Ontario in 2017. He holds a BSc (Hons.) with a double major in Biology and Chemistry from Brock University where he received the distinguished graduating student award for both the Biology and Chemistry departments. He held an NSERC Canada Graduate Scholarship throughout his PhD, which focused on the structural and metalation properties of apo-metallothioneins. Gordon's current research interests involve developing novel mass spectrometry-based techniques for the characterization of disordered proteins.

 This journal is © The Royal Society of Chemistry 2018

Open Access Article. Published on 29 ledna 2018. Downloaded on 14.02.2026 23:30:44.
This article is licensed under a Creative Commons Attribution 3.0 Unported Licence.

lack of secondary and tertiary structures in the metal-free protein means that circular dichroism (CD) spectroscopy is not particularly informative about the apoprotein, and finally because the apoprotein is so dynamic with little formal structure, NMR analysis is precluded.[58] This lack of quantifiable structure has made the establishment of the initial state in the MT metalation pathway difficult. Recently, various mass spectrometric techniques have been employed to overcome the difficulties in studying the apo-MT structure including ion mobility,[59] MS/MS[60] and differential cysteine modification.[57] We now know that at neutral pH the apoprotein adopts a more compact structure, its native structure, under nearly physiological conditions that facilitate faster Cd^{2+} binding kinetics[56] compared to low pH. However, MS data typically do not give detailed information on metal coordination geometry; coordination numbers are left to EXAFS, NMR and X-ray diffraction studies.

Metals commonly associated with MT, including Zn^{2+}, Cd^{2+}, Cu^{+}, Hg^{2+}, and As^{3+}, are coordinated solely by cysteinyl thiols in either digonal, trigonal or tetrahedral coordination geometries. The process of metal binding dramatically changes the structure of this highly dynamic protein. Metal binding introduces new chromophores that facilitate spectroscopic characterization. Most commonly used is the UV-visible absorption spectrum that includes bands in the 220–320 nm region arising from ligand-to-metal charge transfer (LMCT). Also, NMR spectroscopy, both proton and metal based, becomes useful as the metalated protein is far less dynamic than the apo-form. One major issue with a protein that binds multiple metals is that the chromophoric identities of each metal overlap so that the spectral data are the average of all species and are difficult to separate into a stepwise sequence that is necessary for mechanistic analysis. As we will show in this review, ESI-MS data are invaluable in mechanistic studies because all species in the reaction between apo-MT and metals are observed simultaneously. Significantly, the relative concentration can be calculated and used in a traditional manner to obtain binding and rate constants. This means that we are using ESI-mass spectral data in a semi-quantitative manner where calibration anchors the quantitative values. This is much like the use of atomic absorption spectrometry and its reliance on standards.

Optical methods (UV-visible absorption, CD and emission spectroscopy). The first reports on metalated MT involved Cd^{2+} because its LMCT band is located at 250 nm which, in the absence of aromatic amino acids, is easy to measure and became a characteristic marker for Cd-MT in chromatographic separations (K_f-values are listed in the tables below).[3,6] This 250 nm band also identified the formation of the Cd-$(S_{CYS})_n$ metal binding site because of the appearance of a strong chiral band in the CD spectrum.[61] Fig. 1 illustrates well the lack of absorption above 230 nm in rabbit liver apo-MT 2a and the very low absorbance above 240 nm for Zn_7-MT 2A, which together allowed the LMCT thiolate to Cd^{2+} band at 250 nm to be used for quantitatively determining Cd-loading. The CD spectrum adds significantly more information because, unlike the absorbance that increases linearly with Cd-loading up to 7, the CD chirality changes in a non-linear fashion representing the effect of metal-speciation first from the isolated $CdCysS_4$ sites and then from cluster formation on the overall structure of the whole peptide. This is discussed in much more detail towards the end of this review in Section 2.4. It is clearly apparent from the two CD spectra in Fig. 1 that the development of the chiral Cd-S_{CYS} binding site as a function of Cd^{2+} loading (1–7) is quite different. Addition of Cd^{2+} to the apo-MT 2A results in the immediate development of a strong and typical exciton-coupled spectrum arising from the formation of the Cd^{2+}-S_{CYS} cluster that results in 2 pairs of tetrahedrally-coordinated Cd^{2+} in the $[Cd_4(S_{CYS})_{11}]^{3-}$ cluster. The inset shows how the maximum in the chiral signal is centred on 250 nm (note that in the exciton split CD signal the absorption band maximum is at the cross-over point of the CD band). The formation of the α-domain-located cluster is pH dependent and occurs with the first Cd^{2+} added with a pH below 7.0 (see the figures at the end of this review) as described by Irvine *et al.*[52] The remaining 3 Cd^{2+} form stepwise the $[Cd_3(S_{CYS})_9]^{3-}$ β-domain cluster. The lack of exciton coupling means that the CD spectral motif is both weak and centred on the absorption maximum of 250 nm, slightly distorting the spectral envelope.

Martin J. Stillman

Martin Stillman received his B.Sc. and Ph.D. from the University of East Anglia, Norwich, UK under the supervised by Prof. Andrew Thomson, FRS. He worked as a postdoctoral fellow at the University of Alberta, Canada. In 1975, he moved to the University of Western Ontario, where since 1986 he has been Professor of Bioinorganic Chemistry. He is currently Bioinorganic Section Editor-in-Chief with the International Journal of Molecular Sciences. *Martin Stillman is a Fellow of the Canadian Institute of Chemistry. He is the founding Chair of the CanBIC series of Bioinorganic Conferences held in Parry Sound, Ontario every 2 years beginning in 2007. The 7th conference will take place in May 2019. Three areas of research are of current focus: (i) the metal binding mechanism and structural properties in the human protein metallothionein, (ii) the electronic properties of tetrapyrroles and (iii) the mechanism of action of the Isd heme transport proteins in the human pathogenic* Staphylococcus aureus *bacterium. Key tools included ESI-mass spectrometry, CD, magnetic CD, and emission spectroscopy, together with the theoretical methods required to assist interpretation, including molecular dynamics for proteins, and DFT-based techniques for the tetrapyrroles. He has published over 250 papers on these topics. His work is funded by the Natural Sciences and Engineering Research Council of Canada.*

Open Access Article. Published on 29 ledna 2018. Downloaded on 14.02.2026 23:30:44.
This article is licensed under a Creative Commons Attribution 3.0 Unported Licence.

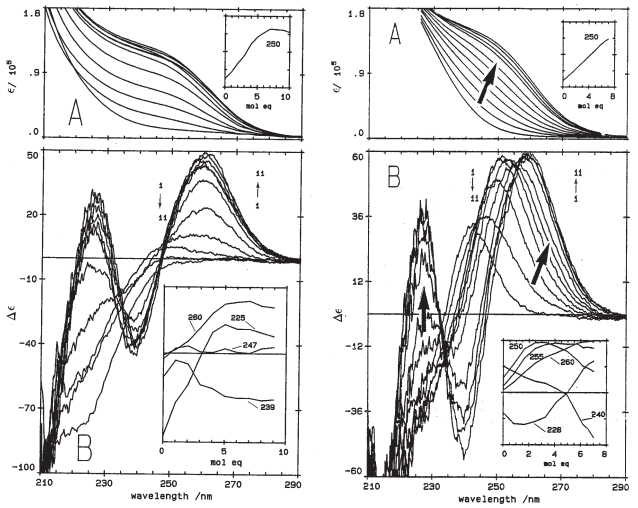

Fig. 1 Absorption (A) and CD (B) spectral data for Cd^{2+} binding to rabbit liver apo-MT 2a and Zn_7-MT 2A at pH 7. (LEFT) Absorption (A) and CD (B) spectral data for Cd^{2+} binding to rabbit liver apo-MT 2a at pH 7. The insets show the change in intensity at each of the wavelengths as a function of Cd^{2+} added. (Right) Absorption (A) and CD (B) spectral data for Cd^{2+} binding to rabbit liver Zn_7-MT 2a at pH 7. The insets show the change in intensity at each of the wavelengths as a function of Cd^{2+} added. The difference in CD spectral patterns is due to the prior presence of Zn^{2+} in the same sites to be occupied by the incoming Cd^{2+}. The distribution of Cd^{2+} between the two domains is reported as a function of relative binding constants in Fig. 20 below. Reproduced from ref. 61 with the permission of the American Society for Biochemistry and Molecular Biology.

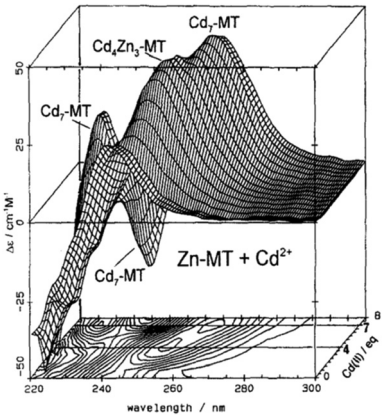

Fig. 2 CD spectra recorded during a titration of rabbit liver Zn_7MT 2a with Cd^{2+} at room temperature and pH 7. The CD spectral data reach a maximum of 4 and 7 Cd^{2+} as indicated by the contour map. Reproduced from ref. 65 with the permission of Wiley and Sons.

The right hand side spectral data show the absorption and CD spectral changes when Cd^{2+} is added to the fully saturated Zn_7MT 2A. Again, the CD spectral data provide wonderful insight into changes taking place in the metal binding regions. The complex CD spectral patterns show that the $[Cd_4(S_{CYS})_{11}]^{3-}$ cluster does not actually form until the very last Cd^{2+} is added. Before that, the spectral bands at each step show that mixed Zn–Cd binding takes place. Only recently with detailed ESI-MS data has the mechanism of this beautiful metal-replacement reaction become clear. Pinter *et al.*[52] reported that the binding constants for each of the 7 sites for the incoming Cd^{2+} were distributed in declining magnitude between both the α and β domains established initially by the 7 Zn^{2+}. The metalation mechanism is quite different when the Zn^{2+} are present. Without the Cd^{2+} binding to apo-MT 2A it would not be obvious what is going on.

CD spectral data provide detailed information during metal titrations of the protein, with the appearance of maxima, minima and isodiochroic points associated with the formation of specific species. The change in protein structure changes the CD spectral intensity whereas the actual chromophore changes the band maximum. Clearly in the data shown in Fig. 1 for Cd^{2+} binding to both apo-MT 2A and the Zn_7-MT 2A, the absorbance at 250 nm simply increases to give a shoulder (on the edge of the peptide absorption of the protein). The CD spectrum on the other hand grows to a single envelope for the apo-MT 2A as discussed above. Fig. 2 shows what happens when Cd^{2+} replaces Zn^{2+} in Zn_7-MT using the 3D view to track the spectral changes seen in Fig. 1 (right). Now there are a series of species that form as the Cd^{2+} replaces Zn^{2+} more or less isostructurally and the band maximum shifts due to the difference in LMCT energy between the two metals. While these data were recorded at room temperature, we have reported that there is a significant temperature dependence when Cd^{2+} is added to Zn_7MT 2A that we assigned to the thermally-induced rearrangement in the peptide chain as a function of the change in cluster dimensions.[61]

These changes in overall structure are far more pronounced when metals that can change their coordination number, and hence geometry, bind to the 20 cysteines of MT. For example, the titration of Cu^{+} into Zn-MT showed the presence of a number of maxima that were associated with the apparent formation of specific stoichiometric minima for $Zn:Cu:S_{CYS}$ in the forming Cu, Zn-MT, Fig. 3. The metalation is highly temperature dependent, with increasing temperatures allowing fast rearrangement to the thermodynamically favorable structures (D).

Similar large changes in the CD spectra as a function of environment are seen with Hg^{2+}, Fig. 4, under 4 different conditions. (A) Hg^{2+} was added to apo-MT 2 at pH 7, showing clear formation of Hg_7-MT 2A, but this (presumably) clustered species collapses with the addition of further Hg^{2+}, forming possibly a stoichiometrically-relevant species with 11 Hg^{2+}. The spectra in (B) confirm the formation of both the 7 and 11 Hg:MT species when Hg^{2+} was added to the Zn_7MT 2A. Here "0" shows the CD spectrum of the Zn_7-MT 2A with a maximum near 230 nm. Like the data shown in Fig. 1, the prearranged or prealigned structure of the MT peptide significantly alters the thermodynamically and kinetically accessible binding sites for the incoming metal. The ionic strength plays an important role as is shown in (C), where at low pH in the presence of high chloride ion concentrations a protein species forms with 18 Hg^{2+} characterized by a very strong CD spectrum that we

 This journal is © The Royal Society of Chemistry 2018

Open Access Article. Published on 29 ledna 2018. Downloaded on 14.02.2026 23:30:44.
This article is licensed under a Creative Commons Attribution 3.0 Unported Licence.

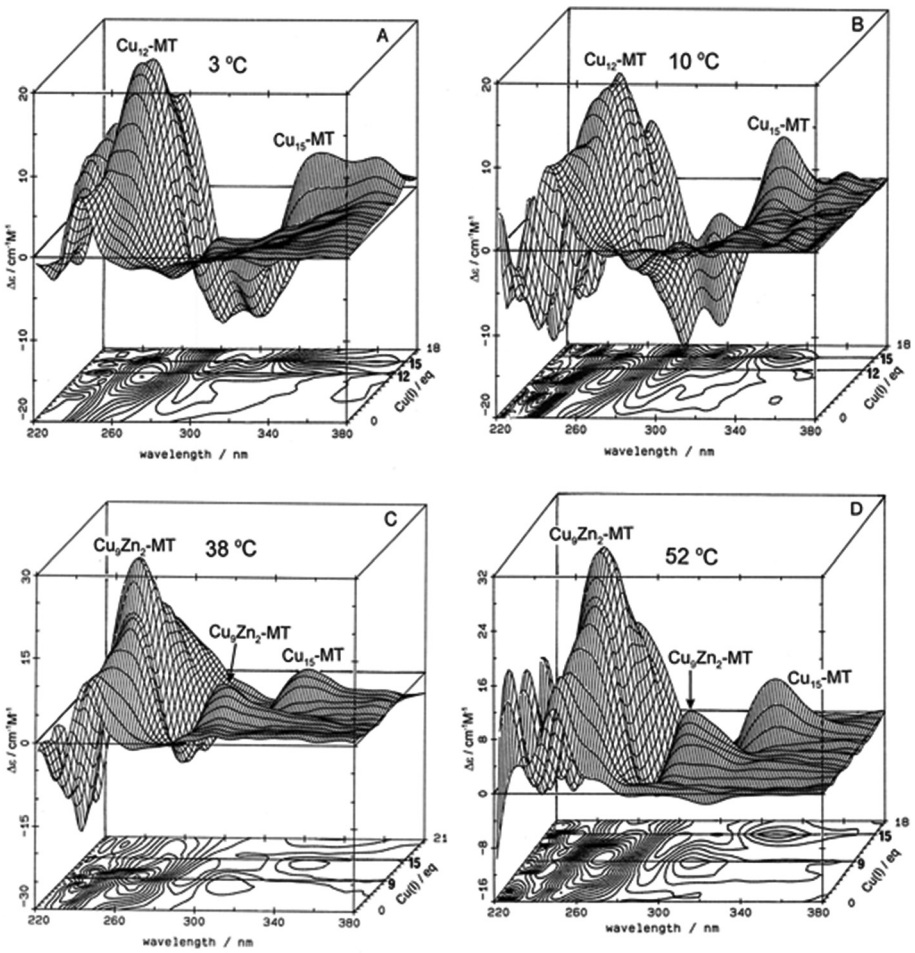

Fig. 3 Temperature dependence of Cu^{+}-thiolate cluster formation in rabbit liver Zn_7-MT 2A. 3-Dimensional projections and the corresponding contour plots of CD spectra recorded during replacement of Zn^{2+} in Zn_7-MT 2a solutions with Cu^{1+} at (A) 3 °C, (B) 10 °C, (C) 38 °C and (D) 52 °C, showing the formation of a range of specific species associated with changes in the coordination number of the existing Cu^{+} as the number of bound metals increases towards 20. Reproduced from ref. 65 with the permission of Wiley and Sons.

assigned as being supermetalated. Much more recently, Rigby-Duncan *et al.*[77] and Sutherland *et al.*[48,78] using CD, ESI-MS and ^{113}Cd NMR methods characterized Cd_5-α MT 1A and Cd_8-MT 1A as supermetallated species. Finally, the solvent also influences MT metalation: in (D) the solvent was changed to 50% glycol and now the Hg^{2+} was added to Zn_7-MT as shown by its strong positive CD spectrum labelled "0" at 230 nm. The Hg^{2+} forms only the Hg_{11}-MT species before the protein unfolds and all structure is lost.[62–64]

The CD spectral data illustrate the complexity of metalation and the difference between the absorption and CD traces illustrates the effect that metal binding has on the orientation of the peptide chain. While the absorption spectrum is dependent on the LMCT band and increases as a function of metal loading, it cannot report on major changes in the structure of the binding site(s). However, CD spectroscopy is sensitive to changes in the wrapping of the peptide around the bound metal – the metal-induced folding described for MT by Duncan & Stillman in 2006.[66] The CD spectral intensity arises from the chirality of the peptide as dictated by the selection of cysteines required to bind each metal with the wavelength dependent on the origin of the electronic transition. For the data reported in Fig. 3, the optical transitions are charge transfer in origin, between the Cu^{+} and the thiolate of the cysteines. The selection of structures is thermodynamically controlled and changes as a function of metal loading as shown in Fig. 3 and 4. Despite assigning at that time specific metal-to-protein ratios with spectral features, results reported much more recently based on detailed, stepwise metal loading experiments monitored by ESI-MS show that for each specific metal : protein ratio, a range of ratios centered on the average metal added exist. The spectral properties are then dominated by the species with the strongest signal, which can distort the analysis. The data described at the end of this review allow more specific assignments to be made. In the end, everything depends on the relative magnitudes of the equilibrium binding constants (where cooperativity requires a larger value compared with the adjacent values) and the spectroscopic motif intensity for each structure formed.

Open Access Article. Published on 29 ledna 2018. Downloaded on 14.02.2026 23:30:44.
This article is licensed under a Creative Commons Attribution 3.0 Unported Licence.

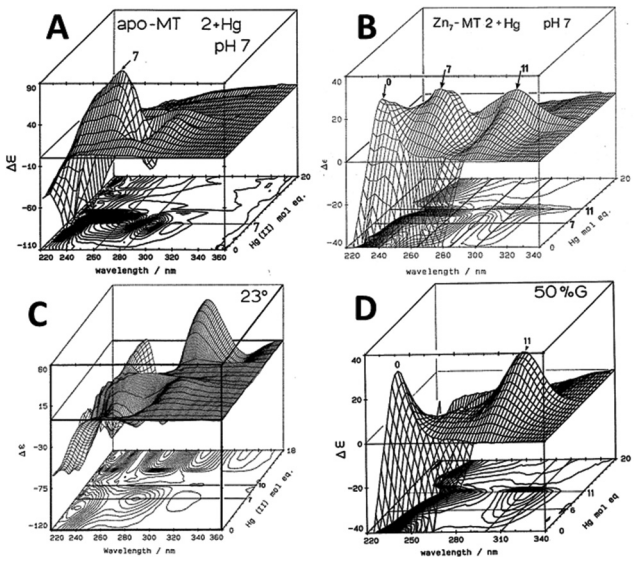

Fig. 4 CD spectral changes recorded during titrations of Hg^{2+} into solutions of rabbit liver apo- and Zn_7-MT 2a (rl-MT 2a) showing the formation of different clustered species. (A) A 3-dimensional representation of the formation of Hg_{18}-rlMT 2a using CD spectra recorded during a titration of a single sample of apo-rlMT 2a with Hg^{2+} at pH 2 and 23 °C in the presence of chloride anions.[64] (B) CD spectra recorded during a titration of Zn_7-rlMT 2a with Hg^{2+} at room temperature and at pH 7. The CD spectra show the loss of Zn_7-rlMT 2a labeled as "0" followed by the formation of Hg_7-rlMT 2a and Hg_{11}-rlMT 2a. (C) A 3-dimensional representation of the formation of Hg_{18}-rlMT 2a using CD spectra recorded during a titration of a single sample of apo-rlMT 2a with Hg^{2+} at pH 2 and 23 °C in the presence of chloride anions.[64] (D) CD spectra recorded during a titration of Zn_7-rlMT 2a with Hg^{2+} at room temperature and at pH 7 in a 50% H_2O/ethylene glycol solvent. The CD spectra show the loss of Zn_7-rlMT 2a labeled "0" followed by the formation of only Hg_{11}-rlMT 2a. Adapted and reproduced from ref. 61 and 63, with the permission of the American Chemical Society.

The CD spectral data shown for Cd^{2+} binding (Fig. 1 and 2), Cu^+ binding (Fig. 3) and Hg^{2+} binding (Fig. 4) clearly demonstrate how the respective metalation reactions with the 20 cysteines of MT 2A involve both different structural motifs (between the beads of isolated metal-thiolate units; see the description of Zn^{2+} and Cd^{2+} binding[52–54]) and clusters. The wavelengths of the band maxima change as a function of the coordination environments of the metal, particularly the coordination number. So, the CD data for the Cd^{2+}-metalation in Fig. 1 and 2 are relatively straightforward, the coordination geometry for beads and clusters remains tetrahedral, but as mentioned above, the CD spectrum is dominated by the electronic exciton coupling between pairs of coordinated Cd^{2+} in the $[Cd_4(S_{CYS})_{11}]^{3-}$ cluster in the α-domain. On the other hand, the coordination geometry for Cu^+ with thiolates is well known to change, with tetrahedral, trigonal and diagonal geometries all reported. Each of these geometries are characterized by charge transfer transitions of different energies, resulting in the CD data of Fig. 3 where the data red shift with the formation of the Cu_{15}-MT species. This clearly (and also logically) indicates the change in coordination geometry from the trigonal expected for Cu_{12}-MT to diagonal. Finally, in the CD data for Hg-MT to be described in Fig. 4, we see an even more dramatic effect of the change in coordination geometry with the Hg : MT ratios of 7, 11 and 18 each resulting in specific structures with individual band maxima and CD motifs. As the number of Hg^{2+} bound increases past 11 Hg : MT (Fig. 4B and D), analysis of the CD spectral data suggests that the size of the formed clusters exceeds the stable conformation, meaning that the structure collapses but still binds Hg^{2+} but not in the well-defined clusters of those "magic numbers",[4] so the chirality is not well-defined either and the CD spectral intensity is, therefore, negligible. However, at an Hg : MT ratio approaching 18 (Fig. 4C), another structure forms with a different band maximum, suggesting another change in coordination geometry with the 18 Hg^{2+} coordinated in a well-defined structure to the 20 cysteines.

We shift now to other spectroscopic methods: first to the use of emission spectroscopy, then NMR, and finally, for the remaining examples, to the remarkable detail of ESI-mass spectral data.

Common use of emission spectroscopy has been limited to Cu-MTs, although there have been reports from Ag-, Pt- and Au-containing MTs.[3,67] The first report by Beltramini and Lerch[68,69] identified the presence of an emission band near 600 nm when a Cu^+ containing MT was excited at 280 nm. This remarkably wide Stokes shift arises from the intersystem crossing populating metal based atomic orbitals. The general nature of the emission properties of Cu-MT was established by many groups and allowed the stoichiometry of Cu : MT to be determined during Cu^+ titrations.[65,70] The emission intensity did not simply increase as a function of Cu^+ loading; rather it increased in a non-linear fashion to a maximum, and then decreased upon further addition of Cu^+. This unusual pattern can be explained by the initial formation of Cu–S clusters that exclude water and, therefore, enhance the long lived excited state population, followed by protein unfolding at high Cu : MT ratios exposing Cu^+ to water. The lifetime of the Cu_n-MT excited state at 600 nm was found to be about 5 microseconds.[71] This short phosphorescence lifetime points to the presence of Cu^+ atomic orbitals as the origin of the emission.[72] It is noteworthy that the emission intensity provides a direct indication of the extent of cluster formation in Cu-MTs. Emission spectroscopy can be used as an indirect measure of the structure since compact cluster structures shielded from the solvent have a high emission intensity compared with the unclustered and solvent exposed conformations. This also implies that each metal must have an individual binding constant (K_f) that represents the incremental stepwise reaction of $Cu_nMT + Cu \rightarrow Cu_{n+1}MT$. However, a more precise method is needed to resolve individual species present in solution and determine the value of these individual K_f's and this is described below using ESI-mass spectral data for these same titrations.

Fig. 5 illustrates the spectral changes that take place with titrations at 2 temperatures.[70] In (A) at 10 °C, a maximum at 12 Cu^+ added to the Zn_7-MT 2 was reached through a steadily

 This journal is © The Royal Society of Chemistry 2018

Open Access Article. Published on 29 ledna 2018. Downloaded on 14.02.2026 23:30:44.
This article is licensed under a Creative Commons Attribution 3.0 Unported Licence.

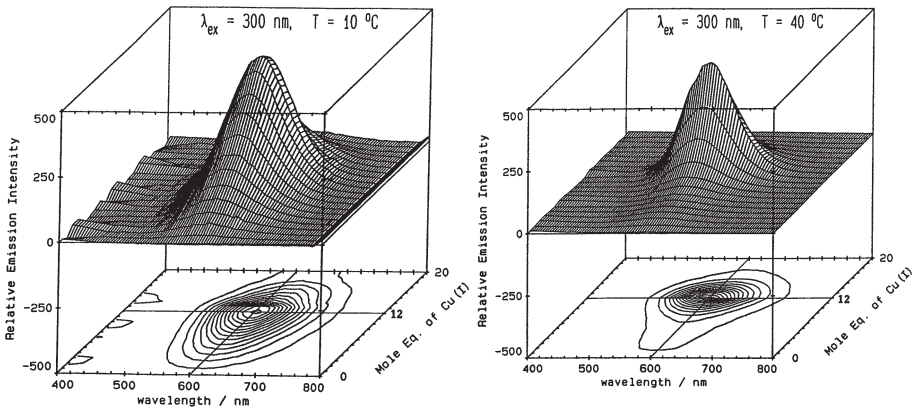

Fig. 5 Emission spectra recorded in the 600 nm region for a titration of rabbit liver Zn_7-MT 2a with Cu^+. (A) Titration at 10 °C shows the gradual intensification of the emission at 600 nm to a maximum at a Cu : MT molar ratio of 12. Addition of Cu^+ results in a loss of intensity. (B) Titration at 40 °C shows a very low emission intensity up to a Cu : MT molar ratio of 6 followed by a rapid increase of intensity to a ratio of 12 following which the intensity drops towards 20 Cu^+ added. Reproduced from ref. 70 with the permission of the American Chemical Society.

increasing signal. However, at 40 °C, the first 6 Cu^+ resulted in very little signal. This was interpreted in the paper as being due to the increased mobility of the Cu^+ so that at low temperatures the Cu^+ was essentially trapped in the kinetic product, whereas at the higher temperatures the Cu^+ could rearrange and that thermodynamic product was not emissive. Exploiting the change in emission intensity, Salgado *et al.*[67] probed the structural properties of Cu^+ in the presence of a competing metal Ag^+. The key to these kinetic studies was that at room temperature the emission recorded is from the Cu–S coordination alone as Ag-S_N only emits at 77 K. The 77 K spectra therefore, were a mixture. These titrations have recently been reported using ESI-MS in parallel to follow the speciation of Cu^+ when added to the 20 cysteines in apo-MT at room temperature.[49]

NMR spectroscopy. Analysis of ^{113}Cd-NMR spectral data first provided evidence for the two clusters of Cd_7MT.[73] Later, analysis of the 2D ^{1}H-NMR data provided the structural information to link the two domains.[74] The orientation of the domains was also established by the single X-ray crystal structure reported in 1991 by Robbins *et al.*[75] Thus, the NMR and X-ray data established the well-known two domain, dumbbell structure of mammalian MTs, which have been recently used as a template for Ag nanoclusters.[76] However, the presence of the two domains dominated the spectral interpretation in a way that may have confused the determination of the metal binding mechanism.

We feel it necessary to emphasize that the clustered domains only exist in MT when the metal loading is high. It appears from experimental data reported to date that there is no mechanism specifically driving metals to any particular coordinating cysteine until clustering is required to accommodate the additional incoming metals.[50] We mean by this that there are thermodynamically favored ratios of metal-to-cysteine that are surprisingly flexible in their values compared with typical metal-binding sites in proteins. Only when the number of metals available to bind to the MT cysteines exceeds the isolated structures possible with cysteines do structures form with different arrangements of bridging cysteinyl thiolates because even then the equilibrium binding constants are still very high. MS–MS data are likely the route to determining if there is a single cysteine as the first in apo-MT bound to an incoming metal.

The property of coordinating an additional Cd^{2+} was first reported by Duncan *et al.* for the supermetalated Cd_5-α domain fragment[77] and later by Sutherland *et al.*[78] for the supermetallated Cd_4-β domain fragment emphasizing the flexibility of the MT peptide. The initial confirmation of these NMR reports came from the CD spectrum of the Cd_5-α-MT[77] because the 5th Cd^{2+} was shown not to be a simple adduct on the outside of the $[Cd_4(S_{CYS})_{11}]^{3-}$ cluster because the CD spectral motif for the exciton split bands centered on 250 nm was replaced by a strong CD motif that was itself centered on the 250 nm band maximum of the LMCT band. The CD spectrum for the first few Cd^{2+} in Fig. 1B also identifies the presence of this non-clustered Cd^{2+}. ^{113}Cd-NMR studies coupled with CD spectral data showed that new clusters had formed in the α and β domain fragments. The ^{113}Cd-NMR spectrum of the "supermetalated" Cd_8MT, Fig. 6, illustrates how the protein can rearrange to accommodate an 8th Cd^{2+}, forming a single super cluster under conditions of excess cadmium.[48] Detailed ESI-mass spectral data established that the Cd_8-MT 1A was the dominant species. For each of these new species, molecular modeling provided reasonable structures.

The optical and NMR techniques provided a wealth of information about the metalated MTs and their metalation and demetalation reactions; however, it was clear that these spectroscopic methods report on averages, that is, the spectral data are the sum of the spectral data for all individual species present. To some extent worse, each species will have its own signal intensity so the averaged observed spectra may not and probably do not represent the weighted average of the fractions

Open Access Article. Published on 29 ledna 2018. Downloaded on 14.02.2026 23:30:44.
This article is licensed under a Creative Commons Attribution 3.0 Unported Licence.

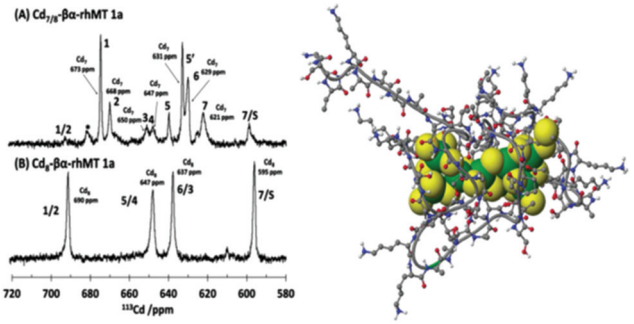

Fig. 6 ^{113}Cd-NMR spectra recorded for (A) Cd_7-rhMT 1a showing the presence of 7 unique sites and (B) Cd_8-rhMT 1a showing the presence of only 4 sites with unique chemical shifts. (C) A proposed structure for the Cd_8-rhMT 1a using a molecular model. Reproduced from ref. 48 with the permission of the American Chemical Society.

of the species present. This ambiguity greatly affects the determination of thermodynamic properties that depend on a specific M : protein ratio. So, the CD spectra recorded during the stepwise addition of Cd^{2+}, Cu^{+}, and Hg^{2+} to Zn_7-MT in Fig. 2–5 are averages. The problem is that we do not have any guide as to the breadth of the averages, so although the overall changes are unambiguous and the final saturated products are understandable, the paths to the final products are not as usable as we would like. Particularly, these data do not allow the determination of the relative individual step binding constants with accuracy or precision. The data described from now on using ESI-MS techniques resolved this problem leading to both kinetic rate constants and equilibrium binding constants. The kinetic data for As^{3+} binding to apo-MT 1A[79,80] firmly established that ESI-MS spectral data could be used in a semiquantitative manner to extract precise binding constants and from there, precise but relative equilibrium binding constants. The extreme of those data are the 20 binding constants for Cu^{+} binding to apo-MT 1A described below, which clearly shows the presence of the cooperatively formed clusters during the stepwise addition of the Cu^{+}.[49]

ESI mass spectrometry. ESI-MS has revolutionized the study of metalloproteins because of its resolving power and the ability to distinguish all species present in solution along with their relative abundance. This is especially useful for the study of MTs where each metalation event can be monitored by the changes in the spectra which correspond to the mass of the metal being investigated. The ionization method is soft, meaning that the energies involved do not fragment the metallocomplex and it is generally believed that the ions detected in the mass spectrum closely match those in the solution. Data presented here from published papers strongly support this view. From these relative abundances, kinetic, equilibria and thermodynamic constants can be determined. Fig. 7 illustrates the details that can be obtained from even a simple titration of metal into a protein. In this titration, Cd^{2+} was added to apo-α-MT 1 at pH 8. As we have shown recently[52] at this pH the Cd^{2+} adds in a distributed fashion forming isolated binding sites (B–E) before forming the clustered Cd_4S_{11}-MT product (F).[81] The presence of all four metalated species at the metal loadings in D and E emphasizes how optical and resonance techniques will record spectra of averages. The data of Irvine and Stillman[52] to be described below clearly account for the observation of the non-cooperatively formed, individually-bound Cd^{2+}, the beads,[54] because cooperative cluster formation only begins to dominate as a mechanistic pathway below pH 7. A less obvious but strikingly important property of the apo-α-MT 2A revealed only through ESI-mass spectra is found in the 1st two spectra, A and B. The apo-α-MT exhibits a maximum charge state at +7, at pH 8. The deconvoluted spectrum (on the right) shows the single mass at 4082 Da of the metal-free MT. The surprising effect of metalation is that with only 0.8 mole equivalents of Cd^{2+} added the charge states are dominated by the +4 species, which remains dominant throughout the metalation. Our explanation is that metalation of the apo-α-MT even by one Cd^{2+} induces folding, reducing the surface area and thereby reducing the dominant charge state to +4. Our interpretation of the missing +7 from the remaining apo-α-MT is that the apo-α-MT associates with the metalated protein and in so doing folds. Confirmation of this interpretation remains for future studies. It does, though, suggest how the apo-MT can survive in the aerobic solutions following translation because the charge state change implies that the protein cysteines will be buried, a conclusion Rigby-Duncan *et al.* came to from modeling and kinetic studies.[81]

The Fenselau group were among the first to apply ESI-MS to metallothioneins in the early 1990s and showed that the method could be used semi-quantitatively.[82] These studies established the use of ESI-MS for the qualitative monitoring of metal exchange and determination of kinetic parameters.[83–85] Thus, the groundwork was laid for a technique that would revolutionize our understanding of the mechanistic details of metal binding by metallothionein.

2.2. Stoichiometry

The original metallated-MTs that were studied in detail were Cd-MTs and the NMR data clearly showed that the stoichiometric ratio was 7 M^{2+} : 1MT. These divalent metals were tetrahedrally coordinated solely by cysteinyl thiols so that the two domains were written as M_3S_9 for the β-domain and M_4S_{11} for the α-domain. The situation was not as clear for Cu^{+} binding because up to 20 Cu^{+} could be seen spectroscopically. Overall, Cu_{12}MT was accepted as the equivalent to the M_7MT of the divalent metals with more than 12 Cu^{+} considered by some to be "supersaturated".[38] The same stoichiometry was assigned to Ag-MT.[86] However, spectroscopic titrations for the last 30 years have suggested that a number of M : MT ratios are possible. Fig. 8 shows the two familiar structures for the Cd_3S_9 and Cd_4S_{11} clusters in the β- and α-domains, respectively, together with the proposed structures found during the titration of Cu^{+} into apo-MT 1,[49] the first formed being Cu_6S_9 in the β-domain, followed by Cu_4S_6 in the α-domain when 10 Cu^{+} had bound, a further 10 Cu^{+} binding finally formed Cu_{20}-MT an unwound loosely folded structure.[49]

 This journal is © The Royal Society of Chemistry 2018

Open Access Article. Published on 29 ledna 2018. Downloaded on 14.02.2026 23:30:44.
This article is licensed under a Creative Commons Attribution 3.0 Unported Licence.

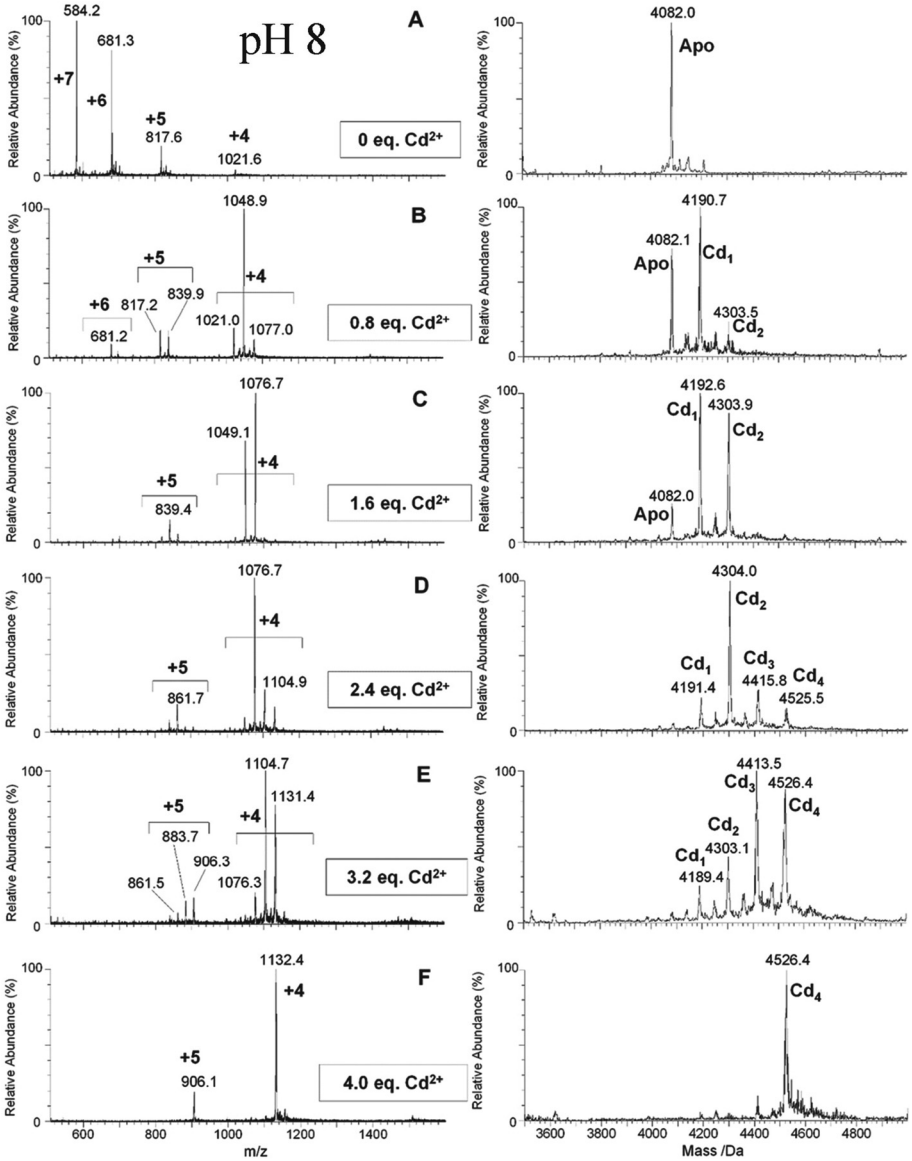

Fig. 7 ESI-MS data recorded during a Cd^{2+} titration of apo-α-rhMT 1a at pH 8. The sequence of A to F shows the change in charge state and deconvoluted parent protein as a function of metalation. At this pH, non-cooperative speciation leads to the formation of Cd_1, Cd_2, Cd_3, and Cd_4. This is particularly clear at this pH in D and E. Reproduced and reprinted from ref. 81 with the permission of John Wiley & Sons, Inc.

In the CD data described above for Hg^{2+}, Fig. 4, we showed that at least 3 different clustered structures can form when Hg^{2+} is titrated into the apo-protein. Table 1 summarizes the reported stoichiometric ratios for a range of MT species and metals. While the mammalian proteins have 20 cysteines, MTs from other organisms have varying numbers of cysteines and we have noted this in the table. Also, while the mammalian MTs bind using cysteines, metal binding in plant and bacterial MTs can involve histidine coordination.[87–89] It is clear from the data extracted from the published reports that many M : MT ratios are possible and the most convincing are those determined by ESI-MS because exact masses of all species in solution are obtained. Spectroscopic titrations rely on careful sequential addition of metals which can be inaccurate due to precipitation and oxidative reactions. It should also be noted that in optical spectroscopy, solution averages are measured and using analytical techniques such as atomic absorption and ICP-OES only provides a ratio of the total metal content to an estimate of the protein content without direct connection.

2.3. Kinetics

The reports of the kinetic rate constants by our group have established that important quantitative binding data could be determined from time and temperature resolved ESI-mass spectral data.[79,80] Table 2 shows a summary of the reported rate constants for metal binding to MT.

Up until the establishment of the As^{3+}-MT binding kinetics, it was considered by many that the metals bound at a single

Open Access Article. Published on 29 ledna 2018. Downloaded on 14.02.2026 23:30:44.
This article is licensed under a Creative Commons Attribution 3.0 Unported Licence.

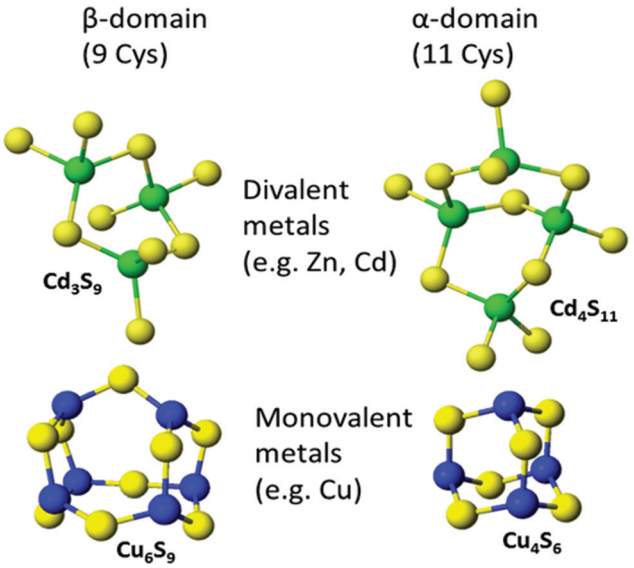

Fig. 8 Well established structures of Cd_3S_9 and Cd_4S_{11} and proposed structures of Cu_6S_9 and Cu_4S_6. Adapted from molecular models based on the X-ray and NMR structures[90,91] and reproduced from ref. 49 with the permission of the Royal Society of Chemistry.

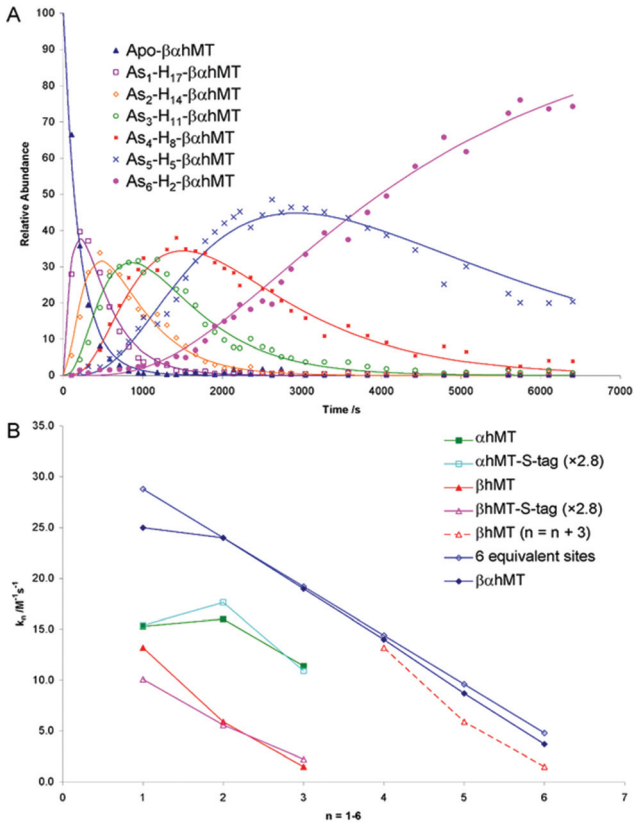

Fig. 9 Time dependent ESI-MS data recorded for As^{3+} binding to rhMT 1a. (A) Time-resolved ESI-MS relative abundances for apo-rhMT 1a following reaction with As^{3+} at 25 °C and pH 3.5 to form As_n-rhMT (n = 1–6). The reaction was carried out with an As^{3+} : MT stoichiometric ratio of 11 : 1. The relative abundances of each of the species are shown as the data points in the graph. The lines were calculated by fitting all the data to a series of sequential bimolecular reactions. (B) Comparison of the rate constants calculated from the time-resolved ESI-MS measurements for As^{3+} metalation of α-rhMT 1a-S-tag, β-rhMT 1a-S-tag, α-rhMT 1a, β rhMT 1a, the full protein βα-rhMT 1a and the trend in rate constant values for 6 equivalent sites where K1 = 28.8 M^{-1} s^{-1}. The dashed line represents rate constant data for the β-rhMT 1a redrawn with the value of n shifted by three illustrating the similarity to the rate constant trend for the final three As^{3+} binding to the βα-rhMT 1a. The protein used was recombinant human (rh) MT 1a. Reproduced from Ngu *et al.* 2008[79] with permission from the American Chemical Society.

rate and with a single binding constant (K_f) in a more or less cooperative fashion. This was due in part to experimental limitations of the stopped-flow spectrophotometers where the complete set of metalation reactions was essentially finished within the dead time of the instrument.[92] The extreme speed in which spectroscopically active metals (such as Cd^{2+} or Cu^{+}) bind to MT made the individual binding kinetics difficult to determine.

The Shaw and Petering groups led in attempts to overcome the difficulty of measuring the fast kinetics of the metal binding reaction to the apo-protein by investigating the demetalation reaction with EDTA, monitored by NMR.[93] In addition, the slower metal exchange between Zn_7-MT and Cd^{2+} was monitored by stopped flow.[94] Furthermore, the kinetics of metal displacement by covalent cysteine modification were also determined.[95] More recent studies by the Russell group showed that metalation/demetalation occurs through very similar pathways yielding identical intermediates in the case of Cd^{2+} binding to human MT 2A.[60]

The kinetics of slower binding metal complexes such as cisplatin were determined in the early 2000s by HPLC, atomic absorption and UV-visible absorption spectroscopy.[96] This paved the way for the study of As^{3+} because its unusually slow binding kinetics was perfectly suited for kinetic analysis by ESI-MS.

The As^{3+} binding data (Fig. 9) showed that the As^{3+} bound sequentially to the full-length protein.[79,80,85] The six rate constants followed a statistical trend where they decrease almost linearly as the binding sites are filled. With no rigid structure defining the binding sites, the incoming metal simply selects a thermodynamically reasonable combination of cysteines to bind to the protein. The rate constant trend can be associated directly with a trend in the six equilibrium binding constants, the K_f-, when we assume that the off-rate is similar for each arsenic. When $K_f = k_{on}/k_{off}$ and k_{off} is constant, the trend in k_{on} is the same as that in K_f. In the data reported for As^{3+}, it was clear that the first As^{3+} bound with a much greater K_f than the last. The distinction between individual binding constants has more important biological significance for zinc and copper where donation to metalloenzymes is governed by the weakest individual binding constant and not the average binding constant of M_xMT (x = 7 M^{2+}, 12 M^{+}). The importance of the kinetic results for As^{3+} with respect to our group's work to determine binding constants cannot be overstated. The individual rate constants fell on a well-defined trend line for the 3 As^{3+} binding steps to the two

 This journal is © The Royal Society of Chemistry 2018

Open Access Article. Published on 29 ledna 2018. Downloaded on 14.02.2026 23:30:44.
This article is licensed under a Creative Commons Attribution 3.0 Unported Licence.

Table 1 Reported stoichiometric data for the metalation of individual species' metallothioneins

Metal	Organism (No. of Cys in sequence)	Isoform	Fragment/ protein	Stoichiometry	Geometry	Technique	Reference
Ag	Rabbit (20)	MT2	βα	$Ag_{18}MT$		CD	86
As	Human (20)	MT1a	α	As_3MT	Trigonal	ESI-MS	80
	Human (20)	MT1a	β	As_3MT	Trigonal	ESI-MS	80
	Rabbit (20)	MT2	βα	As_6MT $(CH_3As)_{10}MT$ $[(CH_3)_2As]_{20}MT$	Trigonal Diagonal Monodentate	ESI-MS	102
Au	Horse kidney (20)	MT	βα		Linear	Chromatographic separation, AAS	103
Bi	Not specified	Not specified	Not specified	Bi_7MT	Tetrahedral	CD, MCD, absorption	104
	Rabbit (20)		βα	Bi_7MT		UV-Vis ICP-AES	105
Cd	Human (20)	MT1a	α	Cd_4MT	Tetrahedral	ESI-MS	106
	Human (20)	MT1a	β	Cd_3MT	Tetrahedral	ESI-MS	106
	Human (20)	MT1a	βα	Cd_7MT	Tetrahedral	ESI-MS	106
	Chickpea (14)	MT2		Cd_5MT		UV-Vis, CD, MCD, ESI-MS, MALDI-TOF	107[a]
	Chickpea (12)	MT1		Cd_4MT Cd_5MT		UV-Vis, CD, FTIR, ESI-MS	108[a]
	Garden pea (12)	MT1		$Cd_{3.9}MT$ $Cd_{5.8}MT$		AAS, SDS-PAGE	109[a]
	Garden pea (12)	MT1		$Cdx MT$ (x = 5.6–6.1)		SDS-PAGE, FPLC	110[a]
	Wheat	E_c-1	Full-length	Cd_6E_c-1	Tetrahedral	UV-Vis, ESI-MS, F-AAS	111, MS 89
	Wheat	E_c-1	γ	$Cd_2γ$-E_c-1	Tetrahedral	ESI-MS, UV-Vis, NMR, F-AAS	112
	Wheat	E_c-1	$β_E$	$Cd_4β_E$-E_c-1	Tetrahedral	ESI-MS, F-AAS	89
	Durum wheat (12)	MT1		$Cdx MT$ ($x = 4 \pm 1$)		UV-Vis, X-ray, MM/MD, SDS-PAGE	113[a]
	Cork oak (14)	MT2		$Cd_{6.3}MT$		ICP-OES, ESI-MS	114[a]
	Grey mangrove (14)	MT2		Cd_3MT		SDS-PAGE, AAS	115[a]
	Banana (10)	MT3		Cd_4MT		UV-Vis, AAS, ESI-MS	116[a]
Co	Rabbit (20)	MT1	βα	Co_7MT	Tetrahedral	MCD, ESR	117
	Rabbit (20)	MT2	βα	Co_7MT	Tetrahedral	UV-Vis	92
	Rabbit (20)	MT2	βα	Co_7MT	Tetrahedral	NMR	118
	Chickpea (14)	MT2		Co_5MT		UV-Vis	107
Cu	Human (20)	MT3	βα	$Cu_{10}MT$		ESI-MS, CD	119
	Human (20)	MT3	β	Cu_6MT		ESI-MS, CD	119
	Human (20)	MT3	α	Cu_4MT		ESI-MS, CD	119
	Human (20)	MT1a	βα	$Cu_{20}MT$	$1Cu : 1S_{Cys}$	ESI-MS	49
	Chickpea (12)	MT1		Cu_6MT Cu_9MT		UV-Vis, CD	120
	Chickpea (14)	MT2		Cu_6MT $Cu_{10}MT$		UV-Vis, CD	120
	Chickpea (14)	MT2		Cu_8MT		UV-Vis, CD, MCD, ESI-MS, MALDI-TOF	107[a]
	Chickpea (12)	MT1		Cu_6MT Cu_9MT		UV-Vis, CD, FTIR, ESI-MS	108[a]
	Garden pea (12)	MT1		$Cu_{2.3}MT$ $Cu_{6.2}MT$		AAS, SDS-PAGE	109[a]
	Cork oak (14)	MT2		$Cu_{5.5}MT$ ($+Zn_{1.7}MT$)		ICP-OES, ESI-MS	114[a]
	Grey mangrove (14)	MT2		Cu_4MT		SDS-PAGE, AAS	115[a]
	Wheat	E_c-1	γ	$Cu_2γ$-E_c-1		F-AAS, UV-Vis, CD, luminescence	112
Fe	Rabbit (20)	MT1	βα	Fe_7MT	Tetrahedral	MCD, EPR	121
Hg	Not specified	Not specified	Not specified	Hg_7MT	Tetrahedral	CD, MCD, absorption	104
	Rabbit (20)	MT	βα	$Hg_{18}MT$		CD	64
Ni	Rabbit (20)	MT1	βα	Ni_7MT	Tetrahedral	MCD, ESR	117
Pb	Not specified	Not specified	Not specified	Pb_7MT	Tetrahedral	CD, MCD, absorption	104
	Mouse (20)	MT1	βα	Pb_9MT		ESI-MS	122
	Mouse (20)	MT1	β	Pb_4MT		ESI-MS	122
	Mouse (20)	MT1	α	Pb_5MT		ESI-MS	122
	Human (20)	MT3	βα	Pb_7MT		ITC	123
Pt	Rat liver (20)	MT	βα	$Pt_{10}MT$		EXAFS	124
	Rat liver (20)	MT	βα	$Pt_{4.5}MT$ (cis-DDP) Pt_6MT (trans-DDP)		UV-Vis, radio-immunoassay	125
	Rat liver (20)	MT	βα	Pt_2Zn_{4MT} (cis-DDP)		Chromatographic separation, AAS, covalent Cys modification	126
Rh	Human (20)	MT1a	β	Rh_2MT		ESI-MS	32

Open Access Article. Published on 29 ledna 2018. Downloaded on 14.02.2026 23:30:44.
This article is licensed under a Creative Commons Attribution 3.0 Unported Licence.

Table 1 *(Contd.)*

Metal	Organism (No. of Cys in sequence)	Isoform	Fragment/ protein	Stoichiometry	Geometry	Technique	Reference
Tc	Rabbit liver (20)	MT1	βα	Tc_7MT		UV-Vis, covalent Cys modification	127
	Rabbit liver (20)	MT1	βα	$Tc_{6.2}MT$		UV-Vis, EXAFS	128
U	Cyanobacteria (9)	SmtA		$(UO_2)_3Zn_4MT$	Bidentate	ESI-MS, Cd, ^{1}H NMR, SDS-PAGE	129
Zn	Human (20)	MT1a	α	Zn_4MT	Tetra	ESI-MS	53
	Human (20)	MT1a	β	Zn_3MT	Tetra	ESI-MS	53
	Human (20)	MT1a	βα	Zn_7MT	Tetra	ESI-MS	53
	Wheat	E_c-1	Full-length	Zn_6E_c-1	Tetrahedral	ESI-MS, F-AAS	111
	Wheat	E_c-1	γ	$Zn_2γ$-E_c-1	Tetrahedral	ESI-MS, F-AAS	112
	Wheat	E_c-1	$β_E$	$Zn_4β_E$-E_c-1	Tetrahedral	ESI-MS, F-AAS	89
	Chickpea (14)	MT2		Zn_5MT		UV-Vis, CD, MCD, ESI-MS, MALDI-TOF	107[a]
	Chickpea (12)	MT1		Zn_4MT Zn_5MT		UV-Vis, CD, FTIR, ESI-MS	108[a]
	Garden pea (12)	MT1		$Zn_{5.6}$ MT $Zn_{11.5}MT$		AAS, SDS-PAGE	109[a]
	Cork oak (14)	MT2		$Zn_{3.5}$ MT		ICP-OES, ESI-MS	114[a]
	Grey mangrove (14)	MT2		Zn_3MT		SDS-PAGE, Coomassie blue, AAS	115[a]
	Banana (10)	MT3		$Zn_{3.4}$ MT		UV-Vis, AAS, ESI-MS	116[a]
	Oil palm (10)	MT3A		$Zn_{1.7}MT$		AAS, SDS-PAGE	130[a]

[a] Adopted from ref. 10. Abbreviations: CD, circular dichroism spectroscopy; MCD, magnetic circular dichroism spectroscopy; UV-Vis, ultraviolet-visible absorption spectroscopy; AAS, atomic absorption spectrometry; ESI-MS, electrospray ionization-mass spectrometry; MALDI-TOF, matrix-assisted laser deposition ionization-time of flight; FTIR, Fourier transform infrared spectroscopy; SDS-PAGE, sodium dodecyl sulfate polyacrylamide gel electrophoresis; ICP-AES/OES, inductively coupled plasma–atomic emission spectrometry/optical emission spectroscopy; ESR/EPR, electron spin/paramagnetic resonance spectroscopy; MM/MD, molecular mechanics/molecular dynamics; FPLC, fast protein liquid chromatography; ITC, isothermal titration calorimetry; EXAFS, extended X-ray absorption fine structure; NMR, nuclear magnetic resonance spectroscopy.

isolated domain fragments, for the 6 As^{3+} binding steps to the full 20 cysteines in MT[97,98] and even for the 9 and 10 As^{3+} binding steps to the 27 and 33 cysteines of triple β- and α-MT,[85] respectively. This almost linear trend for the 20 cysteines of the native apo-MT was strong evidence that the apo-MT peptide acted like a multiple-binding site chelator. This meant we should expect, thermodynamically and statistically, that there would be as many binding constants as metals that bound and that these would trend lower unless there were special products that enhanced cooperative behavior. As we show clearly in the next sections, "special" products are indeed formed. When clustered structures are the thermodynamically favored product then the binding constants for those products distort the expected trend to lower values as the number of metals bound increases, or as the number of available sites diminishes. Indeed, the summary of the rate constants in reference[85] (K_f-values are listed in the tables below) is extremely interesting. The rate constants represent the reaction at each step when following a linear trend line. They indicate binding in a similar fashion to fewer and fewer sites, and when there is deviation we can deduce conformational changes occurring. As an example, the binding of the first As^{3+} is associated with a smaller rate constant than subsequent As^{3+}, which we have assessed as being due to the tight wrapping of the metal-free apo-proteins. We have considered this in modelling studies as well.[57,66,99–101]

2.4. Equilibrium binding affinities

The experimental data shown in Tables 1–3 highlight the promiscuous nature of metal binding to MT. What is clear is that there is no specific metal binding site in the traditional sense of a well-formed set of coordinating amino acids that typically accept metals with the same geometry. Examples of this would include Zn^{2+} binding to carbonic anhydrase and the Zn-finger proteins, where the binding site is close to tetrahedral.[132,133]

When binding affinities are discussed with respect to MT, it should be clear that the values do not correspond to a specific site but to the binding of the n^{th} metal to $M_{n-1}MT$, wherever that may take place. The individual binding event may require backbone rearrangement to position coordinating cysteines, especially during cluster formation. As with the kinetic rate constants, binding affinities tend to decrease statistically as more cysteines are occupied by the already bound metals. Unlike the kinetic constants, there are important exceptions to this general trend. These exceptions tend to be for cluster formation which is a thermodynamically favorable process and is often associated with cooperative binding.

Table 3 contains representative binding constants reported for a range of metals and solution conditions. Only recently have individual constants been reported for each metal bound to MT because the determination of an individual K_f required the measurement of each binding step separately. Only ESI-MS methods provide the resolution required to monitor each step

 This journal is © The Royal Society of Chemistry 2018

Open Access Article. Published on 29 ledna 2018. Downloaded on 14.02.2026 23:30:44.
This article is licensed under a Creative Commons Attribution 3.0 Unported Licence.

Table 2 Reported kinetic data for the metalation of individual metallothioneins

Metal	Organism[a]	Isoform	Fragment/ protein	Stoichiometry	Technique	Rate constants (k [M^{-1} s^{-1}])	Reference
As	Human (20)	MT1a	α	As_3MT	ESI-MS	k_1 5.5 k_2 6.3 k_3 3.9	80
	Human (20)	MT1a	β	As_3MT	ESI-MS	k_1 3.6 k_2 2.0 k_3 0.6	80
	Human (20)	MT1a	βα	As_6MT	ESI-MS	k_1 25 k_2 24 k_3 19 k_4 14 k_5 8.7 k_6 3.7	79
Bi	Rabbit	MT2	βα	Bi_7MT	UV-Vis, ^{1}H NMR	k_1 5.8×10^{-3} (Cd displacement) k_2 1.0×10^{-4} (Cd displacement) k_1 7.2×10^{-3} (Zn displacement) k_2 5.9×10^{-5} (Zn displacement)	105
Cd	Human (20)	MT1a	α	Cd_4MT	Stopped flow spectrophotometry	k_{1-4} 60.4 (native) k_{1-4} 3.32 (denatured)	56
	Horse kidney (20)	MT	βα	Cd_7MT	Absorption spectroscopy	2.7×10^{-6} (demetalation by EDTA)	28
	Rabbit (20)	MT2	βα	Cd_7MT	Stopped flow spectrophotometry	pH 4.1 60 ± 10 pH 4.6 140 ± 30 pH 5.1 280 ± 50 pH 5.4 350 ± 100	92
	Rabbit (20)	MT2	α	Cd_4MT	Stopped flow spectrophotometry	pH 4.6 170 ± 60 pH 5.1 350 ± 100 pH 5.4 460 ± 200	92
Zn	Rabbit (20)	MT2	βα	Zn_7MT	Stopped flow spectrophotometry	pH 4.6 10 ± 1 pH 5.2 15 ± 1 pH 5.8 28 ± 2 pH 6.3 43 ± 7 pH 6.6 100 ± 15 pH 7.2 300 ± 100	92
	Rabbit (20)	MT2	α	Zn_4MT	Stopped flow spectrophotometry	pH 6.6 90 ± 10 pH 7.2 230 ± 100 pH 7.5 690 ± 300	92
Pt	Rabbit (20)	MT	βα	Pt_7MT	Atomic absorption spectroscopy, UV absorption, HPLC	0.14 (to apo-MT) 0.75 to Cd/Zn-MT 0.53 to Cd_7MT 0.65 to Zn_7MT	96
Zn	Horse kidney (20)	MT	βα	Zn_7MT	Absorption	Demetalation by EDTA k_1 fast k_2 14.2×10^{-4} k_3 2.0×10^{-4}	28

[a] The number of cysteines in the peptide is shown in parentheses.

of these multi metal binding reactions. In the case of Zn^{2+} binding to apo-MT we can summarize the complete reaction in the following Scheme 1.

In this series of reactions, the spectroscopic chromophore of $Zn(S_{CYS})_4$ is so similar from step to step that we cannot resolve individual Zn^{2+} binding events. Additionally, the ESI-MS data show that there is a distribution of species that coexist except at the very beginning and end of the titration. This means that the spectroscopic data are simply averages and cannot provide the specific resolution required to obtain each individual binding constant. Individual binding constants for the reactions shown in Scheme 1 were determined by an ESI-MS competition experiment between MT and carbonic anhydrase reported by Pinter *et al.*[55] Carbonic anhydrase was used to calibrate the range of K_f values since its own zinc

$$apoMT + Zn^{2+} \overset{K_1}{\rightleftharpoons} Zn_1MT$$
$$Zn_1MT + Zn^{2+} \overset{K_2}{\rightleftharpoons} Zn_2MT$$
$$Zn_2MT + Zn^{2+} \overset{K_3}{\rightleftharpoons} Zn_3MT$$
$$Zn_3MT + Zn^{2+} \overset{K_4}{\rightleftharpoons} Zn_4MT$$
$$Zn_4MT + Zn^{2+} \overset{K_5}{\rightleftharpoons} Zn_5MT$$
$$Zn_5MT + Zn^{2+} \overset{K_6}{\rightleftharpoons} Zn_6MT$$
$$Zn_6MT + Zn^{2+} \overset{K_7}{\rightleftharpoons} Zn_7MT$$

Scheme 1 A series of 7 single step reactions for Zn^{2+} binding to apo-MT at pH 7 showing the individual binding constants K_1–K_7. The values of the individual K's were first reported in ref. 54 and then modified using competition with carbonic anhydrase.[55] Scheme adapted from ref. 50

Open Access Article. Published on 29 ledna 2018. Downloaded on 14.02.2026 23:30:44.
This article is licensed under a Creative Commons Attribution 3.0 Unported Licence.

Table 3 Reported equilibrium binding constant data for the metalation of individual human metallothioneins

Metal	Isoform	Fragment/Protein	Stoichiometry	Technique	Binding constant value (logK)	Reference
Cu	MT2	βα	$Cu_{10}MT$	ESI-MS, pH 7.5	K 14.6	27
	MT1a	βα	$Cu_{20}MT$	ESI-MS[a], pH 7.4	K_1 15.5 K_2 15.0 K_3 14.6 K_4 19.3 K_5 14.6 K_6 18.9 K_7 12.9 K_8 13.1 K_9 13.7 K_{10} 15.5 K_{11} 10.7 K_{12} 11.2 K_{13} 12.9 K_{14} 9.5 K_{15} 9.5 K_{16} 8.6 K_{17} 8.1 K_{18} 7.0 K_{19} 6.1 K_{20} 5.0	49
Pb	MT3	βα	Pb_7MT	ITC, pH 6.0	K_{1-2} 11.7 K_{3-4} 10.2 K_{4-7} 8.7	123
Zn	MT2	βα	Zn_7MT	Fluoresence spectroscopy[b], pH 7.4	K_{1-4} 11.8 K_5 10.45 K_6 9.95 K_7 7.7	131
	MT3	βα	Zn_7MT	ITC, pH 6.0	K_{1-4} 10.8 K_5 10.5 K_6 9.9 K_7 7.7	123
	MT1a	βα	Zn_7MT	ESI-MS[c]	K_1 12.35 K_2 12.47 K_3 12.52 K_4 12.37 K_5 12.21 K_6 12.05 K_7 11.80	55

Explanations: [a] Determined by analysis of the pH dependent titration data. [b] Binding strength was determined using competitors and a fluorogenic dye. [c] Binding constant values were determined through competition of zinc binding to carbonic anhydrase.

affinity has been well characterized. Of course, in a competition experiment each protein concentration has to be determined using a method like absorption spectroscopy before mixing since the ionization efficiencies in ESI-MS can differ greatly between peptides.

In the case of Zn^{2+} binding, ESI-MS competition experiments revealed that the first two K_f values are smaller than subsequent values, where ITC and spectroscopic studies had averaged $K1$ or 2–4 values and had not shown this counter intuitive phenomenon. The depression of the initial binding constants was interpreted as resulting from the energetically demanding rearrangement of the folded apo-MT to allow the first metals to bind. Covalent modification, ESI-MS studies[57] and IM-MS[59] confirmed that the apo-protein can exist in a number of conformers, many of which are tightly packed. More ESI-MS results from Irvine *et al.*[52] indicated a further complication in pH dependence of the K_f values, which change drastically around pH 7.0 and 5.0 for Cd^{2+} and Zn^{2+} binding, respectively. Cooperativity has been discussed with reference to the metalation mechanism of MT for 40 years or more. Cooperativity manifests itself as a series of increasing K_f values up to the cooperatively formed product. These increasing values are a consequence of more fundamental underlying factors which may include conformational changes and changes in the chemical nature of the ligand as binding proceeds. We can see this effect in the Cu^+ binding constants in Table 3 where K_4, K_6, K_{10}, and K_{13} are all larger than the surrounding K_f values.

Cooperativity *vs.* non-cooperativity; cluster *vs.* bead. A long-standing discussion regarding the metalation mechanism of MTs concerns the metalation mechanism, *i.e.* whether the metals cooperatively form the clusters identified above, Fig. 9. In this mechanism, there should only be a small abundance of intermediate species formed between the apo- and the clustered metalated species. In mammalian MT, the two cluster structure is well known for divalent Zn and Cd[73,75] and in many spectroscopic studies it has been reported that the metalation of apo-MT results in the direct

 This journal is © The Royal Society of Chemistry 2018

formation of the M_4S_{11} cluster forming the α-domain, followed by the M_3S_9 cluster forming the β-domain as shown in Fig. 10. The implication is that there will be no partially metalated species, M_{1-3}MT or M_{5-6}MT. However, many spectroscopic methods that measure the MS_4 chromophore are not sensitive to the individual metalation states, so disentangling the spectroscopic trend as a function of metalation status was ambiguous. ESI-MS methods show all species in solution and offered a detailed view of the metalation pathways adopted under different conditions. The non-coopera-

Open Access Article. Published on 29 ledna 2018. Downloaded on 14.02.2026 23:30:44.
This article is licensed under a Creative Commons Attribution 3.0 Unported Licence.

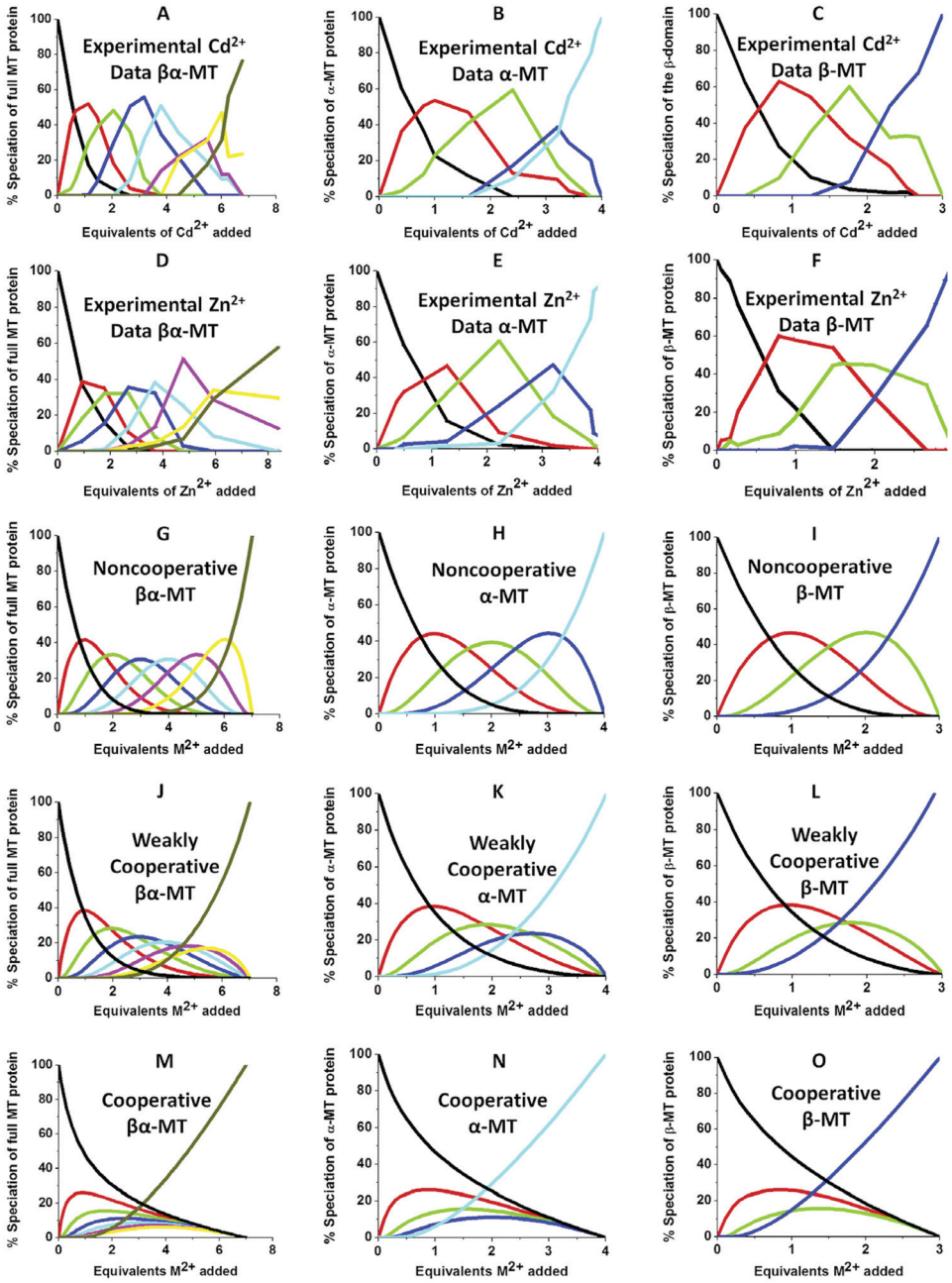

Fig. 10 Experimental ESI-MS data and simulations of ESI-MS data for the metalation of MT and its isolated domains with Cd^{2+} and Zn^{2+}. Models and experimental data showing Cd^{2+} speciation (A–C) and Zn^{2+} speciation (D–F) during metalation of the full MT protein, and the α- and β-domains. A non-cooperative model (declining K_f's) of ESI-MS data based on a series of linearly decreasing association constants (G–I). A weakly cooperative model (equal K_f's) of ESI-MS data based on a series of equal association constants (J–L). A strongly cooperative model (increasing K_f's) of ESI-MS data based on a series of linearly increasing association constants (M–O). The speciation lines are color coded as follows for each of the full protein (A), the α-MT fragment (B), and the β-fragment (C): BLACK – apo-protein, no metals bound; RED – species with 1 Cd^{2+} (A–C) or Zn^{2+} (D–F), or M^{2+} ion (G–O) bound; GREEN – species with 2 metals bound; BLUE – species with 3 metals bound; PALE BLUE – species with 4 metals bound; MAUVE – species with 5 metals bound; YELLOW – species with 6 metals bound; BROWN – species with 7 metals bound. Reproduced from ref. 51 with the permission of Elsevier.

Open Access Article. Published on 29 ledna 2018. Downloaded on 14.02.2026 23:30:44.
This article is licensed under a Creative Commons Attribution 3.0 Unported Licence.

tive mechanism is considered to be the normal metalation pathway in which metals simply bind stepwise to one binding site. For MT this would mean that in the full-length protein, 7 species would form sequentially controlled by 7 binding constants as shown in Scheme 1. In the absence of any special effects these binding constants should diminish equally according to the decreased number of available binding sites. Other than the statistical decrease of binding sites, there is no mechanism that actively excludes subsequent binding events. This lack of exclusion mechanism led to the term "non-cooperative" being more commonly used to describe the MT binding mechanism.

We can illustrate the spectral characteristics that would be observed for both cooperative and non-cooperative Zn^{2+} and Cd^{2+} binding to MT for using ESI-MS metal titration data. First, in Fig. 10 [51] (A–O), we show experimental and simulated speciation data based on the measurement of Cd^{2+} (A, B and C) and Zn^{2+} (D, E and F) binding to the full-length protein and to the isolated α- and β-fragments. The experimental data show that in each of the 6 metalation reactions (A–F) that each, individually-metalated species forms in sequence. This means that 7 metalated species are observed for the full-length protein (A and D), 4 for the α-fragment (B and E) and 3 for the β-fragment (C and F). The simulations of three possible mechanisms, (i) non-cooperative formation of the product (G, H and I), (ii) weakly cooperative formation of the product (J, K and L) and (iii) fully cooperative formation of the product (M, N and O), can be used to assess the type of metalation pathway. Clearly, for MT 1A at this pH the experimentally-determined pathways are all non-cooperative. This led us to ask what controls the choice of pathway during the metalation reaction because other researchers had clearly identified the presence of particularly the M_4S_{11} cluster forming cooperatively.[58,134,135] A possible answer was reported by Irvine *et al.* from pH-dependence of the metalation of apo-MT 1A with Zn^{2+} and Cd^{2+}. In Fig. 11 [52] the pH-dependence of the formation of the clustered M_4S_{11} is shown; M_4 cluster formation was dominant at low pH (4.5 for Zn^{2+} and 6.0 for Cd^{2+}). When the pH was increased to >7 the beaded species (M_1–M_5) were observed, indicating that the M_4S_{11} cluster had been replaced, likely by nMS_4 structures (n = 0–4). This pH dependence of the metalation pathways for both Zn^{2+} and Cd^{2+} is summarized in Fig. 12.[52]

Determination of the binding constants for Zn^{2+} binding to MT. For many years the determination of the 7 Zn^{2+} binding constants for MT has proved challenging due to the lack of individually accessible chromophores. Krezel and Maret,[131] through the use of FRET methods, determined 4 K_f values with some being averages of multiple binding constants (7 K_f values should theoretically be obtained). Again, the use of ESI-MS to distinguish individual M_xMT species in solution and their relative abundance has allowed for more precise determinations. Around neutral pH, the metalation proceeds by the non-cooperative pathway. For each Zn^{2+} addition the Normal distribution of Zn_xMT species shifts gradually towards saturated Zn_7MT with each intermediate becoming the most abundant in solution at its corresponding molar equivalent (*i.e.* Zn_3MT is the most abundant after 3 mol. eq. of Zn^{2+} had been added), Fig. 13.[53]

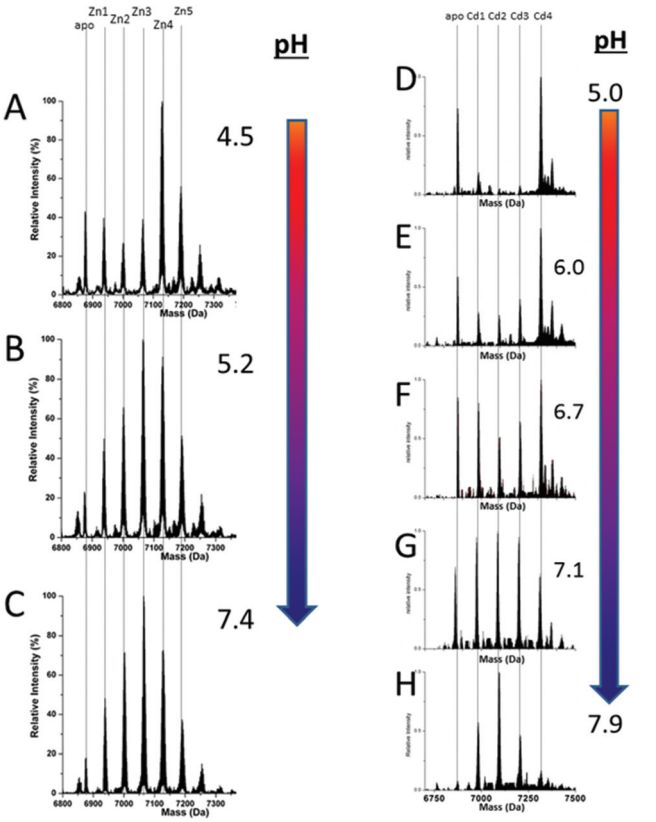

Fig. 11 Changes in speciation of Zn^{2+} and Cd^{2+} binding to apo-rhMT 1a as a function of pH. (A), (B) and (C) ESI-MS data recorded for a single Zn : MT ratio (≈2.5) at pH 4.5, 5.2 and 7.4 showing the redistribution of Zn^{2+} from primarily a clustered Zn_4 species (with a significant fraction of apo-MT remaining) to a series of distributed, non-cooperative species at pH 7.4. (D, E, F, G and H) ESI-MS data recorded for a single Cd : MT ratio (≈2.5) at pH 5.0, 6.0, 6.7, 7.1, and 7.9 showing the redistribution of Cd^{2+} from primarily a clustered Cd_4 species at pH 5 (with a significant fraction of apo-MT remaining) to a series of distributed, non-cooperative species at pH 7.9. Reproduced from ref. 52 with the permission of the Royal Society of Chemistry.

This sequential shift in the species distribution as a function of the mol. eq. of Zn^{2+} added is controlled by the constants of the single step equilibrium reactions (Scheme 1). The solution of this set of 7 reaction equations depends on the initial concentration of the protein, the Zn^{2+} concentration and the values of the 7 binding constants. Previously, it was not possible to separate the speciation at each titration step into individual metalated species, making it impossible to solve for the 7 K_f values. The mass spectral data provided semi-quantitative estimates of the relative concentrations of each species present in solution (Fig. 13). By fitting the abundances of all species to the set of 7 reaction equations we determined the individual K_f values for each step.[54] We then normalized to the average of the values reported by Krezel and Maret.[131] A subsequent 3-way competition between the two fragments and the full-length protein allowed the determination of

 This journal is © The Royal Society of Chemistry 2018

Open Access Article. Published on 29 ledna 2018. Downloaded on 14.02.2026 23:30:44.
This article is licensed under a Creative Commons Attribution 3.0 Unported Licence.

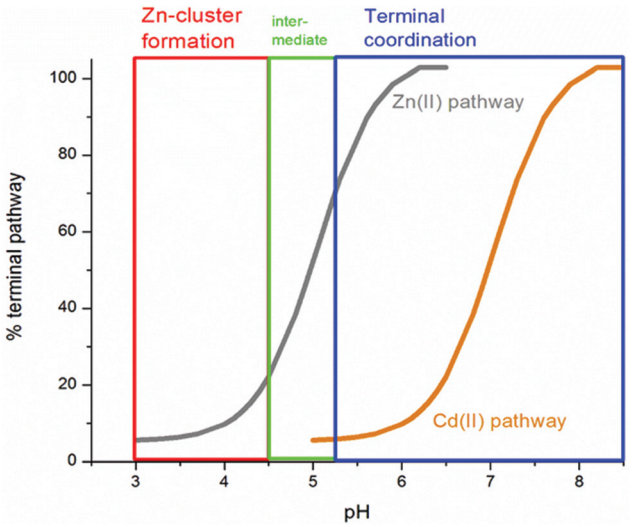

Fig. 12 Summary of the trend in $M_4(S_{CYS})_{11}$ cluster formation as a function of pH for Zn-MT and Cd-MT showing the equilibrium between cooperatively formed clusters at low pH and a distributed, non-cooperatively formed species ("terminal coordination") at neutral pH. Reproduced from ref. 52 with the permission of the Royal Society of Chemistry.

the relative binding constants. The fragments also allowed for the comparison of binding affinities between domains and to quantify the chelation effects of the full-length protein. The quality of the fits can be assessed by a comparison with the simulated speciation based on these same binding constants (Fig. 14 [54]). The important message to take from these experiments is that when competitive chelation occurs, the relative order of the binding constants can be directly determined from the speciation. A very important extra result from this 3-way competition experiment was that the fragment K's exceeded the K's for the full-length protein for the 5th and 6th Zn^{2+}. Our interpretation was that at this point in the stepwise addition of Zn^{2+} the full protein changed from 5 $Zn(S_{CYS})_4^{2-}$ beads to the 2 well-known clusters for the 6th and 7th Zn^{2+}. This massive rearrangement reduced the K_f-values for the full-length protein compared with the isolated fragments. Of course, with different peptides, concentrations must be normalized with a solution-based method, in the case of using the LMCT at 250 nm using Cd^{2+}-remetalation of each peptide and its corresponding extinction coefficient.

Comparing panels A, C, and E in Fig. 14, it is apparent that βα (full-length protein) binds Zn_1 and Zn_2 with binding constants greater than the β- or α-fragments. The K_f values determined by the simulation followed the trend established by the As^{3+} binding kinetics, with a decreasing set of K_f values indicating non-cooperative metalation. However, while the relative K_f values can be determined reliably by ESI-MS and subsequent simulation, the absolute values are more difficult to determine. In this work, we used the average of the 4 values reported by Krezel and Maret[131] as a guide for the approximation of absolute K_f values. We note that the speciation shown in Fig. 14 clearly illustrates the problem of assigning spectroscopic signatures to a specific, single number of metals added to MT. We mean, for example, that the speciation data in Fig. 14 E show that taking a stoichiometric ratio of four for Zn : apo-MT does not mean that Zn_4-MT is the product, rather a Normal distribution of species each controlled by the relative value of K_N. These K values are listed in Table 3.

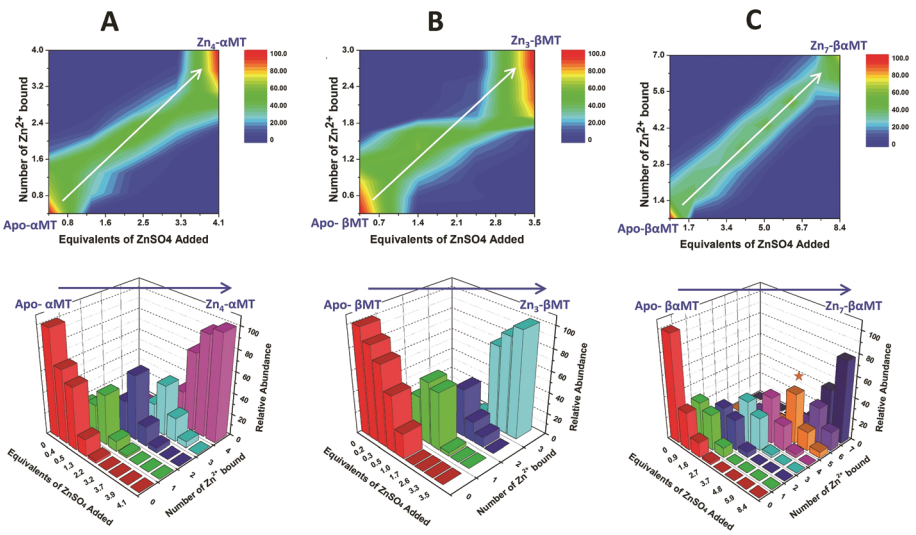

Fig. 13 Representation of the distribution of metalated Zn-species following the non-cooperative pathway, based on analysis of the abundances in the ESI mass spectral data. (A) Zn^{2+} titration of apo-α MT, (B) Zn-titration of apo-β MT and (C) Zn^{2+} titration of apo-MT 1A. The data show the presence of multiple species for every addition of Zn^{2+}. The bar graphs are color coded as follows for each α-MT fragment (A), β-fragment (B) and full protein (C): RED – apo-protein; GREEN – species with 1 Zn^{2+} bound; PURPLE – species with 2 Zn^{2+} bound; BLUE – species with 3 Zn^{2+} bound; PINK – species with 4 Zn^{2+} bound; ORANGE – species with 5 Zn^{2+} bound; MAUVE – species with 6 Zn^{2+} bound; PURPLE – species with 7 Zn^{2+} bound. Reproduced from ref. 53 with the permission of the American Chemical Society.

Open Access Article. Published on 29 ledna 2018. Downloaded on 14.02.2026 23:30:44.
This article is licensed under a Creative Commons Attribution 3.0 Unported Licence.

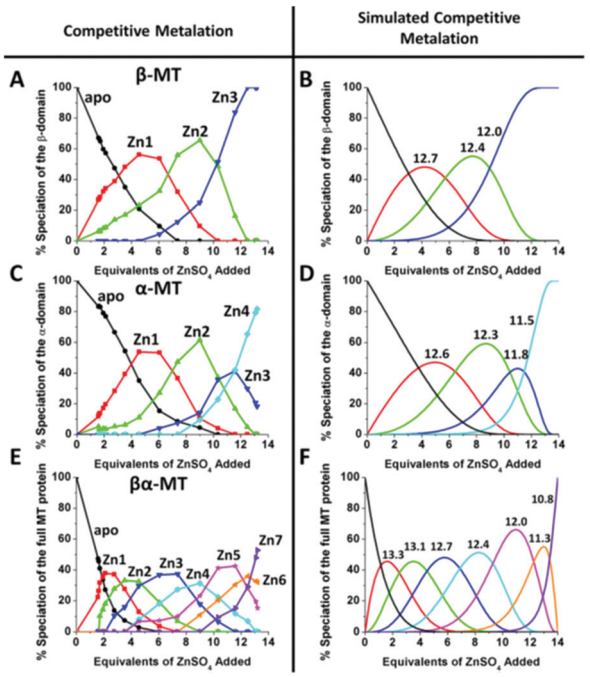

Fig. 14 A 3-way competition between the two fragments and the full-length protein allowed the determination of all the relative binding constants. The two fragments and the full protein were present in the same solution with concentration ratios such that the β-MT provided three binding sites, the α-MT provided 4 binding sites and the βα-protein provided 7 binding sites to give a total of 14 sites. Zn^{2+} was added stepwise and the ESI-MS data were recorded. The ESI-MS data allowed identification of the location of the bound Zn^{2+} as a function of each of the proteins in the same solution. The simulated data are based on a fit of all data using 14 individual binding constants. Reproduced from ref. 54 with the permission of the American Chemical Society.

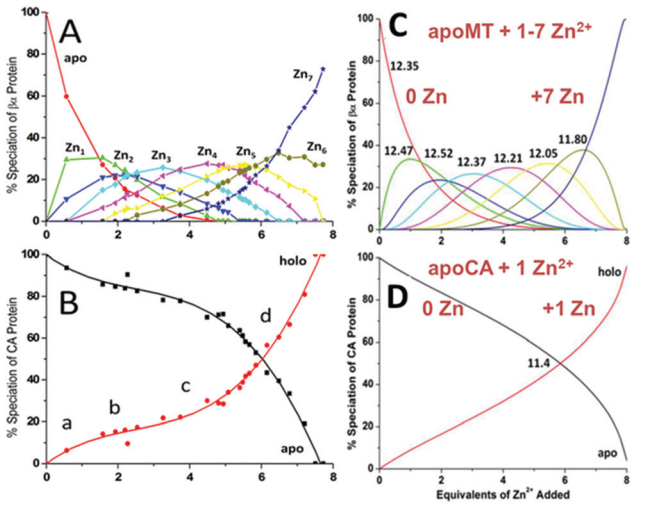

Fig. 15 Two-way competition for Zn^{2+} between apo-rhMT 1a and apo-carbonic anhydrase (CA). ESI mass spectra were recorded as Zn^{2+} was added to equimolar concentrations of apo-rhMT 1a and CA. (A) Zn-MT speciation and (B) Zn^{2+} binding to apo-CA from the ESI-MS data showing the appearance of both Zn_7MT and Zn_1CA (holo-CA) with 8 Zn^{2+} added. (C) and (D) Calculated binding affinities for Zn^{2+} for Zn-MT based on the fixed value of $10^{11.4}$ for Zn^{2+} binding to apo-CA. Reproduced from ref. 55 with the permission of the American Chemical Society.

A more precise method of establishing the absolute K_f values is to use a well-known chelator in direct competition with the protein of interest. Pinter and Stillman[55] used the metalation of carbonic anhydrase (CA) with its known $\log_{10} K_f$ of 11.4 to compete with βα-MT (Fig. 15 [55]). Once again, the clarity of the speciation observed in the MS data immediately identifies the sequence of Zn^{2+} metalation for both MT and CA. In Fig. 15A, CA strongly competes for Zn^{2+} only after Zn_5-MT has formed. To illustrate the competitive binding pattern, the Zn^{2+} contents of the CA and apo-CA were plotted in Fig. 15B. After 6 mol. eq. of Zn^{2+}, CA competes directly with MT for additional Zn^{2+}. Simulations of 8 bimolecular reactions involving 7 sites on MT and one site in CA are shown in Fig. 15C and D. The K_f values determined by this competition experiment are more reliable, as the values are normalized to the $\log_{10} K_f$ of CA. Interestingly, while the last few Zn^{2+} bound have similar K_f values to the data reported by Summers *et al.* (Fig. 14 [54]) the first Zn^{2+} bound to MT in the presence of CA binds with a K_f an order of magnitude smaller ($10^{13.3}$ *vs.* $10^{12.35}$). MS data reported by Irvine and Stillman[136] showed that following partial metalation of apo-α MT with As^{3+} both the metalated protein and the metal-free protein adopted a folded conformation even under denaturing conditions. Based on this result, Pinter and Stillman concluded that in the presence of CA, the metallothionein binding constants may be modified due to protein–protein interactions compared with those in the absence of an interacting partner. Our overall conclusion is that the span of the Zn^{2+} K_f-values ranged down one hundred-fold from approximately $10^{12.5}$ to $10^{10.5}$ and this is the essence of homeostatic control of Zn^{2+} in the cell. The role of MT in providing Zn^{2+} for Zn-dependent enzymes, as demonstrated by the competition with CA, is combined with the homeostatic buffering role which requires binding constants that are out of reach of the enzyme. Fig. 14 and 15 [54] summarize these roles.

Fig. 16 is a complicated diagram that depicts the control exerted by the 7 K_f's on the competitive Zn^{2+} binding between apo-MT 1a and CA when both are present in equal concentrations. The Figure shows through the smooth line in (B) how the fractional metalation of CA only finished when close to 5 Zn^{2+} have bound to the apo-MT 1A. The smooth line shows the fraction of Zn^{2+} that binds to either the apo-MT 1a (high on the *y*-axis) or CA (low on the *x*-axis), where the CA is fully metalated at 1.0 on the *x*-axis. These properties are summarized in Fig. 17 where the five individually bound Zn^{2+} exhibit the largest K_f's, and the two final Zn^{2+} bound result in the 2-domain structure involving bridging cys-thiolates and lower K_f's.

Determination of the binding constants for Cu^+ binding to MT. Cu^+ binding to MT represents the second homeostatic role MT plays. Only Cu^+ binds to the thiolate groups in MT, Cu^{2+} oxidizes the thiolates resulting in disulfide formation and the remaining thiolates binding the reduced Cu^+. The inorganic

 This journal is © The Royal Society of Chemistry 2018

Open Access Article. Published on 29 ledna 2018. Downloaded on 14.02.2026 23:30:44.
This article is licensed under a Creative Commons Attribution 3.0 Unported Licence.

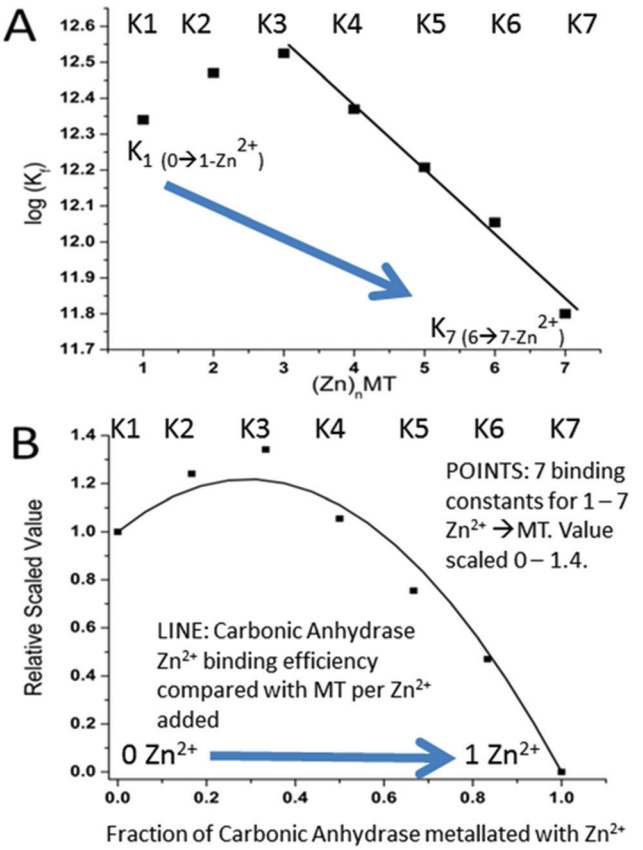

Fig. 16 Schematic representation describing how the seven binding constants for the 7 Zn^{2+} bound to apoMT1a control the competitive uptake of the single Zn^{2+} by Carbonic Anhydrase (CA) when Zn^{2+} is added to a mixture of apo-MT 1A and CA. (A) The 7 binding constants calculated from the simulation shown in Fig. 15 as a function of the number of Zn^{2+}'s bound, 1–7. (B) Superposition of (i) (POINTS) the 7 binding constants calculated from the simulation shown in Fig. 15 as a function of the number of Zn^{2+}'s bound, 1–7, and scaled on the *x*-axis between 0 and 1.4 and on the *y*-axis between 0 and the complete metalation of CA (*y*-axis = 1.0). (ii) (SMOOTH LINE) The fraction of Zn^{2+} bound to apo-MT (*y*-axis scaled 0–1.4) and to CA (*x*-axis scaled 0.0–1.0) after each Zn^{2+} was added in a stepwise fashion. The data show that the first 4 Zn^{2+} primarily bind to the MT. CA only binds a significant fraction of the added Zn^{2+} once 5 Zn^{2+} have bound to the apo-MT 1A. Reproduced from ref. 55 with the permission of the American Chemical Society.

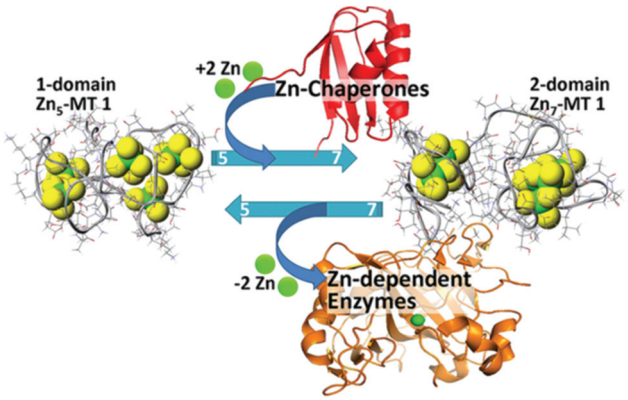

Fig. 17 Schematic representation of the speciation in Zn-MT 1a showing the change between 5 individually bound Zn^{2+} "beads" from the non-cooperative pathway to the two domain structure formed with 7 Zn^{2+} illustrating the interaction between the Zn-MT and Zn-chaperones and Zn-dependent enzymes at physiological pH. Reproduced from ref. 54 with the permission of the American Chemical Society.

chemistry of Cu^{+} thiolates involves digonal, trigonal, and tetrahedral coordination as well as a wide array of clustered species.[137–140] This means that when the 20 cysteines of MT bind to Cu^{+}, a variety of structures can be formed due to the multiple possible coordination geometries and the flexible peptide backbone. Like the ZnS_4, the individual CuS_n (n = 2–4) chromophores are not easily distinguishable spectroscopically for the determination of a stepwise mechanism of Cu^{+} binding. In addition, it is known that up to 20 Cu^{+} will bind to MT, complicating the task of disentangling the single steps.

The most detailed mechanistic information has been reported from emission and CD experiments where Cu_6MT, Cu_9MT, Cu_{12}MT and Cu_{15}MT species resulted in maxima in the spectral data.[65,70] However, other groups reported maxima for Cu_4 and Cu_8MT species[141,142] and the cooperative formation of a mixed metal Cd_3Cu_5MT.[143] As we have described above, a major issue during the titration of any metal into MT is the coexistence of multiple species with different numbers of metals bound. In this context, with the addition of 6 mol. eq. Cu^{+} to MT 1a, species from Cu_4 to Cu_9 are observed in the mass spectrum.[49] That means that spectroscopic methods are not sensitive enough to the specific metal-to-MT stoichiometry and will report intensities based on the average speciation in solution. CD, absorption and emission methods indicate changes in band centers and intensities but the average always blurs the signature of the individual species. The best optical results are obtained when there is a substantial change in chromophore properties. For example, the folding of the protein to form Cu^{+} clusters results in significant intensification of the emission due to the exclusion of water, which quenches Cu^{+} emission. When the protein unfolds at large Cu : MT molar ratios, the interaction with water molecules quenches the emission. Similarly, in the CD spectrum, changes in speciation that result in changes in the chiral peptide surrounding the metal centers as a result of the refolding of the peptide around a cluster are the most easily observed transitions.[65]

The complexity of Cu^{+} binding is shown in Fig. 18 [49] where the results of the simulation of the mass spectral data are shown. The mass spectral data for the Cu^{+} titration were analyzed in terms of 20 consecutive bimolecular reactions (Scheme 2). For a non-cooperative pathway, we would expect a series of species to form with a Normal distribution around the mean mol. eq. of Cu^{+} added, as seen in Fig. 18A. For a cooperative pathway, we would expect formation of species with specific Cu : MT ratios. The emission and CD data suggested that there would be clustered species formed, likely cooperatively. It was apparent from the mass spectral data that specific species formed with greater abundance, and these

Open Access Article. Published on 29 ledna 2018. Downloaded on 14.02.2026 23:30:44.
This article is licensed under a Creative Commons Attribution 3.0 Unported Licence.

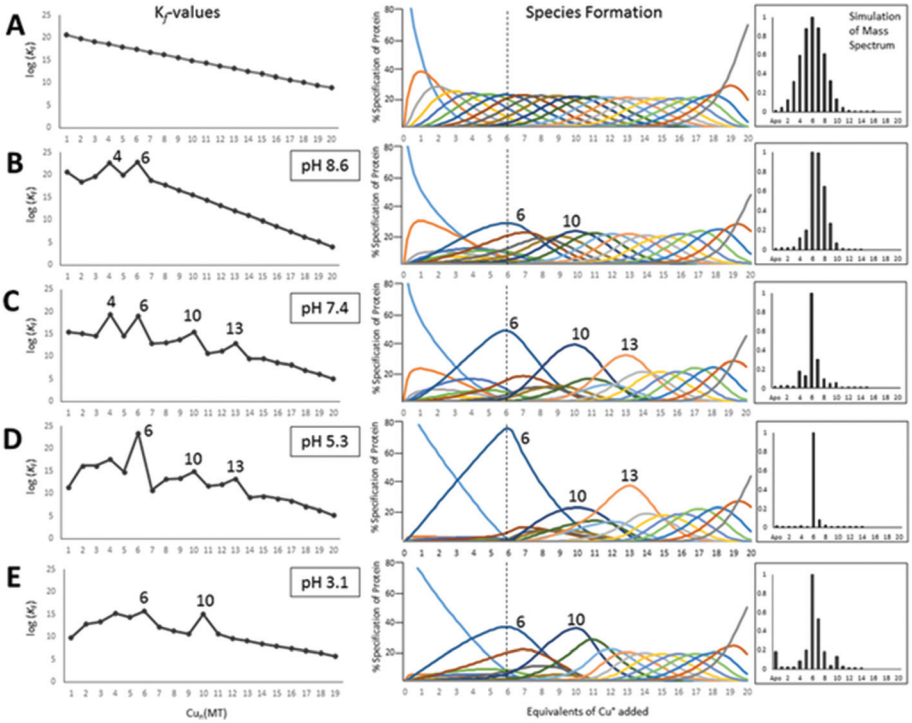

Fig. 18 Results of fitting a series of 20 consecutive bimolecular reactions linked by their respective binding constants (Scheme 2) to the experimental ESI-mass spectral data recorded for titrations of apo-rhMT1a with up to 20 Cu^+ at pH 8.6, 7.4, 5.3 and 3.1. The left column shows the trend in the individual K_f values as a function of Cu^+ loading, the middle column shows individual species formation, and the right column shows a simulated mass spectrum at the titration point of 6 mol. eq. Cu^+ added for each pH-value. The top row (A) shows the simulation based on 20 declining K_f values that would be expected when Cu^+ binds in a completely non-cooperative manner with no cluster formation. (B)–(E) show the fitted binding constants for the stepwise copper binding reactions at the range of pH's. Cooperative cluster formation changes as a function of the pH. The cluster formation dominates the speciation numbered 6, 10, and 13. Reproduced from ref. 49 with the permission of the Royal Society of Chemistry.

$$
\begin{aligned}
apoMT + Cu^{1+} &\overset{K_1}{\rightleftharpoons} Cu_1MT\\
Cu_1MT + Cu^{1+} &\overset{K_2}{\rightleftharpoons} Cu_2MT\\
Cu_2MT + Cu^{1+} &\overset{K_3}{\rightleftharpoons} Cu_3MT\\
Cu_3MT + Cu^{1+} &\overset{K_4}{\rightleftharpoons} Cu_4MT\\
Cu_4MT + Cu^{1+} &\overset{K_5}{\rightleftharpoons} Cu_5MT\\
Cu_5MT + Cu^{1+} &\overset{K_6}{\rightleftharpoons} Cu_6MT\\
&\vdots\\
Cu_{19}MT + Cu^{1+} &\overset{K_{20}}{\rightleftharpoons} Cu_{20}MT
\end{aligned}
$$

Scheme 2 20 bimolecular reactions of Cu^+ binding to MT. Adapted from ref. 49.

species corresponded to clusters previously indicated. However, at higher molar ratios of Cu^+, a Normal distribution was observed. Our conclusion was that Cu^+ binding to MT involved a mixture of cooperative formation of clusters at lower Cu : MT ratios and non-cooperative binding of Cu^+ at higher ratios in isolated sites involving one or two cysteine residues.

The HySS simulation program was used to fit the ESI-MS experimental data using 20 K_f values.[49] Fig. 18 shows that the 4 cooperatively formed species dominate the spectra and simulation (the Cu_4, Cu_6, Cu_{10}, and Cu_{13} species). It is likely that first a Cu_4S_6 cluster is formed, which then forms a Cu_6S_9 cluster in the β-domain. At 10 mol. eq. of Cu^+ two clusters form, Cu_6S_9 in β and Cu_4S_6 in α and at 13 mol. eq. the Cu_4S_6 cluster expands to Cu_7S_{11} (with Cu_6S_9 still in β). The fitted data clearly show that past the Cu_{13} point Cu^+ is bound non-cooperatively. The simulated species formation in Fig. 18 also accounts for the optical properties previously reported. It should be noted that the oft-cited Cu_{12} species, which is thought to have 6 Cu in each of the domains, did not feature prominently in the ESI-MS results. It is possible that the previous interpretation of the optical data mistook a mixture of Cu_{10} and Cu_{13} species for Cu_{12} when 12 mol. eq. of Cu was added to the MT. Another possibility includes isoform specific cluster preferences and variation between MTs obtained from different sources (*i.e.* from different mammals).

We do recognize that the data in Fig. 18 represent a biologically unlikely set of reactions. It is not suggested that *in vivo* 20 Cu^+ bind to apo-MT, rather the significance in the data shown in Fig. 18 and described fully in ref. 49 is clearly showing how the cooperative formation of clusters is dependent on the pH and that the structural properties are fluxional – different pathways are followed depending on the environment (pH), temperature, and metalation status. Dogmatically assigning cluster formation to MT is not correct; clusters form when it is a thermodynamic product. As the Zn^{2+}-binding studies showed,

 This journal is © The Royal Society of Chemistry 2018

Open Access Article. Published on 29 ledna 2018. Downloaded on 14.02.2026 23:30:44.
This article is licensed under a Creative Commons Attribution 3.0 Unported Licence.

bead-formation takes place at physiological pH up to 5 Zn^{2+} added, only then do the 6th and 7th Zn^{2+} added result in the rearrangement to the two-domain, clusters of the X-ray and NMR structures. In other words, the 2 last sites only exist because those metals that can use bridging thiolates can increase the metal loading in that way. The supermetalated Cd_8-MT is just the next phase as the 2-cluster structure is lost and a single structure forms.[48,77]

Domain specificity: metalation of the apo-MT. Determining the location of the individual metals during stepwise metalation of apo-MT is difficult. We chose to determine the location of the metals binding the full-length protein by examining the competitive metalation of the two isolated fragments as Zn^{2+} and Cd^{2+} that were added to a solution containing equimolar amounts of the fragments. In this experiment, the ESI mass spectral data at pH 7.4 follows a non-cooperative pathway and shows the individual sites of each metal bound. Fig. 19 [50] shows the analysis of the mass spectral data in terms of selectivity between the two fragments. Fig. 19A and C indicate that at pH 7.4 there is little domain specificity with the first metal binding fractionally more to the β-domain than the α-domain. Between 2 and 5 metals added, the α-domain is slightly preferred because the α-domain binds 4 metals compared to 3 for the β-domain. The conclusion reached was that at pH 7.4 for the MT 1A protein there would be minimal domain specificity with a non-cooperative metalation pathway. The situation is quite different at lower pH (5.8); thus, following initial occupancy of the β-domain, the α-domain dominates as a result of the cooperative formation of the M_4S_{11} cluster. The conclusion is that at lower pH there would be domain specificity for the full-length apoprotein with the α-domain dominating due to cooperative cluster formation.

Domain specificity: competition of Cd^{2+} for Zn^{2+} sites. A more common question concerns the domain specificity during the competition for Zn^{2+} sites by Cd^{2+}. Fig. 20 [50] outlines the different intertwined pathways for complete replace-

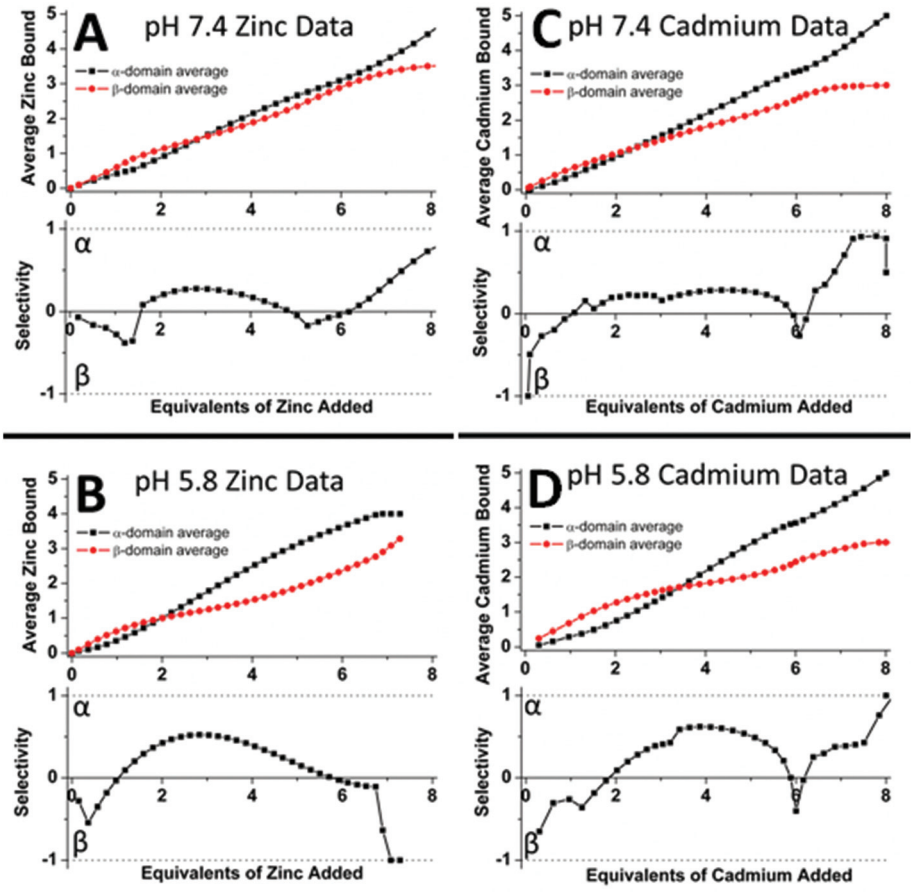

Fig. 19 Analysis of the experimental ESI-MS data for Zn^{2+} (A, B) and Cd^{2+} (C, D) titrations of equimolar solutions of the α- and β-domain fragments showing the distribution of the Zn^{2+} and Cd^{2+} between the two domain fragments as a function of pH. The average Zn^{2+} bound graphs (top in A and B) and the average Cd^{2+} bound graphs (top in C and D) show the weighted distribution of the metal in the specified fragment (domain). The selectivity of each stepwise-added Zn^{2+}/Cd^{2+} as a function of the pH is shown in the lower panels where if the data are negative this means that the Zn^{2+}/Cd^{2+} are preferentially located in the β-fragment whereas if the data are positive the Zn^{2+}/Cd^{2+} are preferentially located in the α-fragment. The graphs show that fragment (domain) selectivity is minimal at pH 7.4 (the dotted line is close to the "0" line until the 4th metal that has to bind to the α-domain fragment) but α is preferred at pH 5.8 for both metals (the dotted line is clearly above the "0" line for the 2–4 metal-added stages). Reproduced from ref. 50 with the permission of the American Chemical Society.

Open Access Article. Published on 29 ledna 2018. Downloaded on 14.02.2026 23:30:44.
This article is licensed under a Creative Commons Attribution 3.0 Unported Licence.

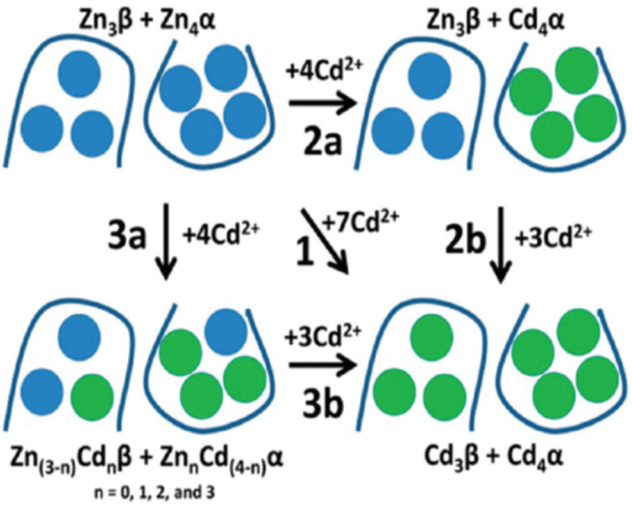

Fig. 20 Schematic representation of the domain choices in the binding site for Cd^{2+} when binding to Zn_7-βα rhMT1a. Pathway 1 implies complete replacement of Zn^{2+} by Cd^{2+} with no stepwise placement identified; pathway 2a shows cooperative formation of $[Cd_4S_{11}]^{3-}$ in the α-domain; pathway 3a shows a distributed binding of Cd^{2+} forming mixed Zn^{2+}/Cd^{2+} clusters in both domains, followed by Pathway 3b with saturation of both domains. The associated binding constant data supported Pathways 3a and 3b: that is, non-cooperative displacement of Zn^{2+}. Reproduced from ref. 50 with the permission of the American Chemical Society.

ment of Zn^{2+} by Cd^{2+}, for the full-length protein. Pathway 2a represents the cooperative, domain specific formation of Cd_4S_{11}. Pathway 3a shows the non-cooperative, non-domain specific displacement of 4 Zn^{2+} by Cd^{2+}. The ESI mass spectral data recorded at pH 5.8 show that neither Zn^{2+} nor Cd^{2+} binding follows a domain selective binding mechanism when Cd^{2+} is added to the Zn^{2+} saturated domain fragments. This means that the binding affinity constants for the two metals span both fragments in their magnitude, resulting in a distribution of metals as indicated in Pathway 3a.

3. Conclusions

Our goal in this very personal review was to summarize our laboratory's decades-long progress towards an understanding of the metal binding mechanism of mammalian MTs and the subsequent internal rearrangements. First, we should restate that the major property of the majority of MTs is that they bind multiple metals into well-defined binding sites when saturated with metals. However, the lack of specificity in both metal identity, binding site location and even geometry has complicated the determination of mechanistic details. This ambiguity has arisen from the overlap in metalation status and the lack of significant and individual differences in the chromophoric properties of each of the several possible metals when bound. The clearest data were reported by X-ray diffraction studies and ^{113}Cd-NMR and ^{1}H-NMR results. However, these data were from the metal saturated proteins which meant that the stoichiometry, cluster formation and coordination geometry were well defined, but that the mechanism involved in the stepwise binding into those sites was not available.

The many spectroscopic studies involving a variety of optical methods indicated that metalation is accompanied by changes in the peptide, but the overlap of chromophores blurred the determination of specific speciation during stepwise binding. Clarity on the stepwise binding mechanism was delivered by ESI mass spectral data. The report on the kinetics of As^{3+} binding outlined each metalation step and the effect of the declining availability of cysteines on the rate constants was understood. For the purposes of determining binding affinities it was necessary to separate the speciation such that each equilibrium reaction could also be defined. The As^{3+}-binding kinetics provided evidence that the binding affinities should decline as a function of metal loading. This then led to the determination of the effect of cooperativity on the binding affinities. The cooperative formation of clusters was well known, but the effect on the remaining metalation reactions up to saturation was not well described. The ESI mass spectral data provided the details necessary to incorporate both cooperative, cluster-driven pathways and non-cooperative, distributed pathways into the overall mechanistic description of MT metalation. These developments have led us to the complete analysis of Cu^{+} binding to apo-MT with its 20 binding constants. In a sense, the unraveling of the complex metalation pathways of metallothionein and its role in cellular chemistry has really only just begun. We look forward to detailed mechanistic details of the major metals involved *in vivo* and an understanding of the environmental factors controlling the metalation status and, therefore, the homeostatic and redox roles of metallothioneins.

Conflicts of interest

There are no conflicts to declare.

Acknowledgements

We gratefully acknowledge financial support from the NSERC of Canada through Discovery and Research Tools and Instruments Grants (to M.J.S.) and a Canada Graduate Scholarship (CGS-D) to G.W.I. We also thank Prof. Andrea Hartwig (KIT, Germany) for a highly productive collaboration that allowed Ms Scheller to work in M.J.S.'s laboratory in 2016 and 2017. M.J.S. thanks the many students who have worked on and have maintained their interest in the metallothionein projects for the last 20 years; without your dedication and perseverance the latest results described here would not have been possible. We thank Ms. A. Zhang for the Table of Contents graphics that, we hope, shows the properties of metallothionein gradually coming into focus since the first reports of 1957. We wish to also acknowledge Mr Doug Hairsine, who has continued to provide excellent technical

 This journal is © The Royal Society of Chemistry 2018

assistance with the mass spectrometer for many years. Our work could not be carried out without the continued excellence of the electronic, computational and mechanical support of all our instruments over many years from Mr John Vanstone and the team members of the Department of Chemistry Electronics Shop. We thank Dr Eva Freisinger for data on the wheat proteins. We also acknowledge and thank the anonymous reviewers who provided many insightful and valuable comments.

Open Access Article. Published on 29 ledna 2018. Downloaded on 14.02.2026 23:30:44.
This article is licensed under a Creative Commons Attribution 3.0 Unported Licence.

References

1 C. A. Blindauer, *Chem. Commun.*, 2015, **51**, 4544–4563.
2 C. A. Blindauer and O. I. Leszczyszyn, *Nat. Prod. Rep.*, 2010, **27**, 720–741.
3 M. J. Stillman, *Coord. Chem. Rev.*, 1995, **144**, 461–511.
4 D. E. Sutherland and M. J. Stillman, *Metallomics*, 2011, **3**, 444–463.
5 D. E. Sutherland and M. J. Stillman, *Metallomics*, 2014, **6**, 702–728.
6 M. Margoshes and B. L. Vallee, *J. Am. Chem. Soc.*, 1957, **79**, 4813–4814.
7 L. Vergani, M. Grattarola, C. Borghi, F. Dondero and A. Viarengo, *FEBS J.*, 2005, **272**, 6014–6023.
8 O. I. Leszczyszyn, H. T. Imam and C. A. Blindauer, *Metallomics*, 2013, **5**, 1146–1169.
9 E. Freisinger, *Dalton Trans.*, 2008, 6663–6675.
10 E. Freisinger, *J. Biol. Inorg. Chem.*, 2011, **16**, 1035–1045.
11 C. D. Klaassen and J. Liu, *Drug Metab. Rev.*, 1997, **29**, 79–102.
12 G. K. Andrews, *Biochem. Pharmacol.*, 2000, **59**, 95–104.
13 E. Tokuda, S.-I. Ono, K. Ishige, A. Naganuma, Y. Ito and T. Suzuki, *Toxicology*, 2007, **229**, 33–41.
14 N. O. Nartey, J. V. Frei and M. G. Cherian, *Lab. Invest.*, 1987, **57**, 397–401.
15 S. Somji, M. A. Sens, D. L. Lamm, S. H. Garrett and D. A. Sens, *Cancer Detect. Prev.*, 2000, **25**, 62–75.
16 A. Miles, G. Hawksworth, J. Beattie and V. Rodilla, *Crit. Rev. Biochem. Mol. Biol.*, 2000, **35**, 35–70.
17 B. A. Masters, C. J. Quaife, J. C. Erickson, E. J. Kelly, G. J. Froelick, B. P. Zambrowicz, R. L. Brinster and R. D. Palmiter, *J. Neurosci.*, 1994, **14**, 5844–5857.
18 C. J. Quaife, S. D. Findley, J. C. Erickson, G. J. Froelick, E. J. Kelly, B. P. Zambrowicz and R. D. Palmiter, *Biochemistry*, 1994, **33**, 7250–7259.
19 Y. Kojima, C. Berger, B. L. Vallee and J. Kägi, *Proc. Natl. Acad. Sci. U. S. A.*, 1976, **73**, 3413–3417.
20 K. Balamurugan and W. Schaffner, *Biochim. Biophys. Acta*, 2006, **1763**, 737–746.
21 S. Lutsenko, *Curr. Opin. Chem. Biol.*, 2010, **14**, 211–217.
22 C. M. St.Croix, K. J. Wasserloos, K. E. Dineley, I. J. Reynolds, E. S. Levitan and B. R. Pitt, *Am. J. Physiol.: Lung Cell. Mol. Physiol.*, 2002, **282**, L185–L192.
23 D. J. Ecker, T. R. Butt, E. J. Sternberg, M. P. Neeper, C. Debouck, J. A. Gorman and S. T. Crooke, *J. Biol. Chem.*, 1986, **261**, 16895–16900.
24 G. Isani and E. Carpene, *Biomolecules*, 2014, **4**, 435–457.
25 S. R. Sturzenbaum, O. Georgiev, A. J. Morgan and P. Kille, *Environ. Sci. Technol.*, 2004, **38**, 6283–6289.
26 G. Meloni, V. Sonois, T. Delaine, L. Guilloreau, A. Gillet, J. Teissie, P. Faller and M. Vasak, *Nat. Chem. Biol.*, 2008, **4**, 366–372.
27 L. Banci, I. Bertini, S. Ciofi-Baffoni, T. Kozyreva, K. Zovo and P. Palumaa, *Nature*, 2010, **465**, 645–648.
28 T.-Y. Li, A. J. Kraker, C. F. Shaw and D. H. Petering, *Proc. Natl. Acad. Sci. U. S. A.*, 1980, **77**, 6334–6338.
29 G. Meloni, P. Faller and M. Vasak, *J. Biol. Chem.*, 2007, **282**, 16068–16078.
30 A. Krezel and W. Maret, *Biochem. J.*, 2007, **402**, 551–558.
31 B. Ruttkay-Nedecky, L. Nejdl, J. Gumulec, O. Zitka, M. Masarik, T. Eckschlager, M. Stiborova, V. Adam and R. Kizek, *Int. J. Mol. Sci.*, 2013, **14**, 6044–6066.
32 D. L. Wong and M. J. Stillman, *Chem. Commun.*, 2016, **52**, 5698–5701.
33 E. Atrian-Blasco, A. Santoro, D. L. Pountney, G. Meloni, C. Hureau and P. Faller, *Chem. Soc. Rev.*, 2017, **46**, 7683–7693.
34 J. H. Kägi and B. L. Vallee, *J. Biol. Chem.*, 1960, **235**, 3460–3465.
35 J. H. Kägi and B. L. Vallee, *J. Biol. Chem.*, 1961, **236**, 2435–2442.
36 P. Babula, M. Masarik, V. Adam, T. Eckschlager, M. Stiborova, L. Trnkova, H. Skutkova, I. Provaznik, J. Hubalek and R. Kizek, *Metallomics*, 2012, **4**, 739–750.
37 D. H. Nies, E. Freisinger and G. J. Krauss, *Ecological Biochemistry: Environmental and Interspecies Interactions*, 2014, pp. 236–257.
38 A. Krężel and W. Maret, *Int. J. Mol. Sci.*, 2017, **18**, 1237.
39 M. Vasak, *J. Trace Elem. Med. Biol.*, 2005, **19**, 13–17.
40 J. Kägi, M. Vasák, K. Lerch, D. E. Gilg, P. Hunziker, W. R. Bernhard and M. Good, *Environ. Health Perspect.*, 1984, **54**, 93.
41 M. J. Stillman and A. P. Presta, *Molecular biology and toxicology of metals*, Taylor & Francis, New York, 2000, pp. 276–299.
42 M. J. Stillman, C. F. Shaw and K. T. Suzuki, *Metallothionein: Synthesis, structure, and properties of metallothioneins, phytochelatins, and metal-thiolate complexes*, Wiley-VCH, 1992.
43 G. W. Irvine and M. J. Stillman, *Int. J. Mol. Sci.*, 2017, **18**, 913.
44 J. Chan, Z. Huang, M. E. Merrifield, M. T. Salgado and M. J. Stillman, *Coord. Chem. Rev.*, 2002, **233**, 319–339.
45 T. T. Ngu, M. D. Dryden and M. J. Stillman, *Biochem. Biophys. Res. Commun.*, 2010, **401**, 69–74.
46 T. T. Ngu, S. Krecisz and M. J. Stillman, *Biochem. Biophys. Res. Commun.*, 2010, **396**, 206–212.
47 D. L. Wong, M. E. Merrifield-MacRae and M. J. Stillman, *Lead: Its Effects on Environment and Health*, 2017, vol. 17, p. 241.
48 D. E. Sutherland, M. J. Willans and M. J. Stillman, *J. Am. Chem. Soc.*, 2012, **134**, 3290–3299.

Open Access Article. Published on 29 ledna 2018. Downloaded on 14.02.2026 23:30:44.
This article is licensed under a Creative Commons Attribution 3.0 Unported Licence.

49 J. S. Scheller, G. W. Irvine, D. L. Wong, A. Hartwig and M. J. Stillman, *Metallomics*, 2017, **9**, 447–462.
50 T. B. Pinter, G. W. Irvine and M. J. Stillman, *Biochemistry*, 2015, **54**, 5006–5016.
51 D. E. Sutherland, K. L. Summers and M. J. Stillman, *Biochem. Biophys. Res. Commun.*, 2012, **426**, 601–607.
52 G. W. Irvine, T. B. Pinter and M. J. Stillman, *Metallomics*, 2016, **8**, 71–81.
53 D. E. Sutherland, K. L. Summers and M. J. Stillman, *Biochemistry*, 2012, **51**, 6690–6700.
54 K. L. Summers, D. E. Sutherland and M. J. Stillman, *Biochemistry*, 2013, **52**, 2461–2471.
55 T. B. Pinter and M. J. Stillman, *Biochemistry*, 2014, **53**, 6276–6285.
56 G. W. Irvine, K. E. R. Duncan, M. Gullons and M. J. Stillman, *Chem. – Eur. J.*, 2015, **21**, 1269–1279.
57 G. W. Irvine, M. Santolini and M. J. Stillman, *Protein Sci.*, 2017, **26**, 960–971.
58 M. Good, R. Hollenstein, P. J. Sadler and M. Vasak, *Biochemistry*, 1988, **27**, 7163–7166.
59 S.-H. Chen, L. Chen and D. H. Russell, *J. Am. Chem. Soc.*, 2014, **136**, 9499–9508.
60 S.-H. Chen, W. K. Russell and D. H. Russell, *Anal. Chem.*, 2013, **85**, 3229–3237.
61 M. J. Stillman, W. Cai and A. J. Zelazowski, *J. Biol. Chem.*, 1987, **262**, 4538–4548.
62 W. Cai and M. J. Stillman, *J. Am. Chem. Soc.*, 1988, **110**, 7872–7873.
63 W. Lu and M. J. Stillman, *J. Am. Chem. Soc.*, 1993, **115**, 3291–3299.
64 W. Lu, A. J. Zelazowski and M. J. Stillman, *Inorg. Chem.*, 1993, **32**, 919–926.
65 A. Presta, A. R. Green, A. Zelazowski and M. J. Stillman, *Eur. J. Biochem.*, 1995, **227**, 226–240.
66 K. E. R. Duncan and M. J. Stillman, *J. Inorg. Biochem.*, 2006, **100**, 2101–2107.
67 M. T. Salgado, K. L. Bacher and M. J. Stillman, *J. Biol. Inorg. Chem.*, 2007, **12**, 294–312.
68 M. Beltramini and K. Lerch, *FEBS Lett.*, 1982, **142**, 219–222.
69 M. Beltramini and K. Lerch, *FEBS Lett.*, 1981, **127**, 201–203.
70 A. R. Green, A. Presta, Z. Gasyna and M. J. Stillman, *Inorg. Chem.*, 1994, **33**, 4159–4168.
71 M. J. Stillman, Z. Gasyna and A. J. Zelazowski, *FEBS Lett.*, 1989, **257**, 283–286.
72 M. J. Stillman and Z. Gasyna, *Methods Enzymol.*, 1991, **205**, 540–555.
73 J. D. Otvos and I. M. Armitage, *J. Am. Chem. Soc.*, 1979, **101**, 7734–7736.
74 B. A. Messerle, A. Schaffer, M. Vasak, J. H. R. Kagi and K. Wuthrich, *J. Mol. Biol.*, 1990, **214**, 765–779.
75 A. Robbins, D. McRee, M. Williamson, S. Collett, N. Xuong, W. Furey, B. Wang and C. Stout, *J. Mol. Biol.*, 1991, **221**, 1269–1293.
76 S. Hu, B. Ye, X. Yi, Z. Cao, D. Wu, C. Shen and J. Wang, *Talanta*, 2016, **155**, 272–277.
77 K. E. R. Duncan, C. W. Kirby and M. J. Stillman, *FEBS J.*, 2008, **275**, 2227–2239.
78 D. E. Sutherland, M. J. Willans and M. J. Stillman, *Biochemistry*, 2010, **49**, 3593–3601.
79 T. T. Ngu, A. Easton and M. J. Stillman, *J. Am. Chem. Soc.*, 2008, **130**, 17016–17028.
80 T. T. Ngu and M. J. Stillman, *J. Am. Chem. Soc.*, 2006, **128**, 12473–12483.
81 K. E. Rigby-Duncan and M. J. Stillman, *FEBS J.*, 2007, **274**, 2253–2261.
82 X. Yu, M. Wojciechowski and C. Fenselau, *Anal. Chem.*, 1993, **65**, 1355–1359.
83 J. Zaia, D. Fabris, D. Wei, R. L. Karpel and C. Fenselau, *Protein Sci.*, 1998, **7**, 2398–2404.
84 Y. Hathout, D. Fabris and C. Fenselau, *Int. J. Mass Spectrom.*, 2001, **204**, 1–6.
85 T. T. Ngu, J. A. Lee, T. B. Pinter and M. J. Stillman, *J. Inorg. Biochem.*, 2010, **104**, 232–244.
86 A. J. Zelazowski and M. J. Stillman, *Inorg. Chem.*, 1992, **31**, 3363–3370.
87 C. A. Blindauer, M. T. Razi, D. J. Campopiano and P. J. Sadler, *J. Biol. Inorg. Chem.*, 2007, **12**, 393–405.
88 O. I. Leszczyszyn, R. Schmid and C. A. Blindauer, *Proteins: Struct., Funct., Genet.*, 2007, **68**, 922–935.
89 E. A. Peroza, R. Schmucki, P. Guntert, E. Freisinger and O. Zerbe, *J. Mol. Biol.*, 2009, **387**, 207–218.
90 D. A. Fowle and M. J. Stillman, *J. Biomol. Struct. Dyn.*, 1997, **14**, 393–406.
91 A. Presta, D. A. Fowle and M. J. Stillman, *J. Chem. Soc., Dalton Trans.*, 1997, 977–984, DOI: 10.1039/A605462E.
92 J. Ejnik, J. Robinson, J. Zhu, H. Försterling, C. F. Shaw and D. H. Petering, *J. Inorg. Biochem.*, 2002, **88**, 144–152.
93 T. Gan, A. Munoz, C. F. Shaw-III and D. H. Petering, *J. Biol. Chem.*, 1995, **270**, 5339–5345.
94 J. Ejnik, C. F. Shaw-III and D. H. Petering, *Inorg. Chem.*, 2010, **49**, 6525–6534.
95 C. F. Shaw III, L. He, A. Muñoz, M. M. Savas, S. Chi, C. L. Fink, T. Gan and D. H. Petering, *J. Biol. Inorg. Chem.*, 1997, **2**, 65–73.
96 D. Hagrman, J. Goodisman, J. C. Dabrowiak and A.-K. Souid, *Drug Metab. Dispos.*, 2003, **31**, 916–923.
97 T. T. Ngu and M. J. Stillman, *Dalton Trans.*, 2009, 5425–5433.
98 T. T. Ngu and M. J. Stillman, *IUBMB Life*, 2009, **61**, 438–446.
99 K. E. R. Duncan and M. J. Stillman, *FASEB J.*, 2006, **20**, A501–A501.
100 K. E. Rigby, J. Chan, J. Mackie and M. J. Stillman, *Proteins: Struct., Funct., Bioinf.*, 2006, **62**, 159–172.
101 K. E. Rigby and M. J. Stillman, *Biochem. Biophys. Res. Commun.*, 2004, **325**, 1271–1278.
102 G. Jiang, Z. Gong, X.-F. Li, W. R. Cullen and X. C. Le, *Chem. Res. Toxicol.*, 2003, **16**, 873–880.
103 G. Schmitz, D. Minkel, D. Gingrich and C. Shaw, *J. Inorg. Biochem.*, 1980, **12**, 293–306.
104 W. Bernhard, M. Good, M. Vašák and J. H. Kägi, *Inorg. Chim. Acta*, 1983, **79**, 154–155.

 This journal is © The Royal Society of Chemistry 2018

Open Access Article. Published on 29 ledna 2018. Downloaded on 14.02.2026 23:30:44.
This article is licensed under a Creative Commons Attribution 3.0 Unported Licence.

105 H. Sun, H. Li, I. Harvey and P. J. Sadler, *J. Biol. Chem.*, 1999, **274**, 29094–29101.
106 D. E. K. Sutherland and M. J. Stillman, *Biochem. Biophys. Res. Commun.*, 2008, **372**, 840–844.
107 X. Wan and E. Freisinger, *Metallomics*, 2009, **1**, 489–500.
108 O. Schicht and E. Freisinger, *Inorg. Chim. Acta*, 2009, **362**, 714–724.
109 A. M. Tommey, J. Shi, W. P. Lindsay, P. Urwin and N. J. Robinson, *FEBS Lett.*, 1991, **292**, 48–52.
110 P. Kille, D. R. Winge, J. L. Harwood and J. Kay, *FEBS Lett.*, 1991, **295**, 171–175.
111 E. A. Peroza and E. Freisinger, *J. Biol. Inorg. Chem.*, 2007, **12**, 377–391.
112 J. Loebus, E. A. Peroza, N. Blüthgen, T. Fox, W. Meyer-Klaucke, O. Zerbe and E. Freisinger, *J. Biol. Inorg. Chem.*, 2011, **16**, 683.
113 K. Bilecen, U. H. Ozturk, A. D. Duru, T. Sutlu, M. V. Petoukhov, D. I. Svergun, M. H. Koch, U. O. Sezerman, I. Cakmak and Z. Sayers, *J. Biol. Chem.*, 2005, **280**, 13701–13711.
114 G. Mir, J. Domènech, G. Huguet, W.-J. Guo, P. Goldsbrough, S. Atrian and M. Molinas, *J. Exp. Bot.*, 2004, **55**, 2483–2493.
115 G.-Y. Huang and Y.-S. Wang, *Aquat. Toxicol.*, 2010, **99**, 86–92.
116 E. Freisinger, *Inorg. Chim. Acta*, 2007, **360**, 369–380.
117 M. Vasak, J. H. Kaegi, B. Holmquist and B. L. Vallee, *Biochemistry*, 1981, **20**, 6659–6664.
118 I. Bertini, C. Luchinat, L. Messori and M. Vasak, *J. Am. Chem. Soc.*, 1989, **111**, 7296–7300.
119 E. Artells, O. Palacios, M. Capdevila and S. Atrian, *FEBS J.*, 2014, **281**, 1659–1678.
120 X. Wan, O. Schicht and E. Freisinger, *Z. Anorg. Allg. Chem.*, 2013, **639**, 1365–1369.
121 M. Good and M. Vasak, *Biochemistry*, 1986, **25**, 8353–8356.
122 Ò. Palacios, À. Leiva-Presa, S. Atrian and R. Lobinski, *Talanta*, 2007, **72**, 480–488.
123 M. C. Carpenter, A. S. Shah, S. DeSilva, A. Gleaton, A. Su, B. Goundie, M. L. Croteau, M. J. Stevenson, D. Wilcox and R. N. Austin, *Metallomics*, 2016, **8**, 605–617.
124 A. Pattanaik, G. Bachowski, J. Laib, D. Lemkuil, C. Shaw, D. Petering, A. Hitchcock and L. Saryan, *J. Biol. Chem.*, 1992, **267**, 16121–16128.
125 A. J. Żelazowski, J. S. Garvey and J. D. Hoeschele, *Arch. Biochem. Biophys.*, 1984, **229**, 246–252.
126 A. Kraker, J. Schmidt, S. Krezoski and D. Petering, *Biochem. Biophys. Res. Commun.*, 1985, **130**, 786–792.
127 M. Morelock, T. Cormier and G. Tolman, *Inorg. Chem.*, 1988, **27**, 3137–3140.
128 W. B. Jones, T. E. Elgren, M. M. Morelock, R. Elder and D. E. Wilcox, *Inorg. Chem.*, 1994, **33**, 5571–5578.
129 C. Acharya and C. A. Blindauer, *Inorg. Chem.*, 2016, **55**, 1505–1515.
130 S. N. A. Abdullah, S. Cheah and D. J. Murphy, *Plant Physiol. Biochem.*, 2002, **40**, 255–263.
131 A. Krezel and W. Maret, *J. Am. Chem. Soc.*, 2007, **129**, 10911–10921.
132 N. J. Pace and E. Weerapana, *Biomolecules*, 2014, **4**, 419–434.
133 D. W. Christianson and C. A. Fierke, *Acc. Chem. Res.*, 1996, **29**, 331–339.
134 P. M. Gehrig, C. You, R. Dallinger, C. Gruber, M. Brouwer, J. H. R. Kagi and P. E. Hunziker, *Protein Sci.*, 2000, **9**, 395–402.
135 J. Byrd and D. R. Winge, *Arch. Biochem. Biophys.*, 1986, **250**, 233–237.
136 G. W. Irvine and M. J. Stillman, *Biochem. Biophys. Res. Commun.*, 2013, **441**, 208–213.
137 R. A. Himes, G. Y. Park, A. N. Barry, N. J. Blackburn and K. D. Karlin, *J. Am. Chem. Soc.*, 2007, **129**, 5352–5353.
138 R. Pufahl, C. Singer, K. Peariso, S.-J. Lin, P. Schmidt, C. Fahrni, V. C. Culotta, J. Penner-Hahn and T. O'halloran, *Science*, 1997, **278**, 853–856.
139 V. Martin-Diaconescu, K. N. Chacón, M. U. Delgado-Jaime, D. Sokaras, T.-C. Weng, S. DeBeer and N. J. Blackburn, *Inorg. Chem.*, 2016, **55**, 3431–3439.
140 E. W. Dahl and N. K. Szymczak, *Angew. Chem., Int. Ed.*, 2016, **55**, 3101–3105.
141 D. L. Pountney, I. Schauwecker, J. Zarn and M. Vasak, *Biochemistry*, 1994, **33**, 9699–9705.
142 B. Roschitzki and M. Vašák, *Biochemistry*, 2003, **42**, 9822–9828.
143 M. Vaher, N. Romero-Isart, M. Vašák and P. Palumaa, *J. Inorg. Biochem.*, 2001, **83**, 1–6.